Assessing the Variability in the Relationship Between the Particulate Backscattering Coefficient and the Chlorophyll a Concentration From a Global Biogeochemical-Argo Database

Marie Barbieux, Julia Uitz, Annick Bricaud, Emanuele Organelli, Antoine Poteau, Catherine Schmechtig, Bernard Gentili, Grigor Obolensky, Edouard Leymarie, Christophe Penkerc'H, et al.

Assessing the Variability in the Relationship Between the Particulate Backscattering Coefficient and the Chlorophyll *a* Concentration From a Global Biogeochemical-Argo Database

Marie Barbieux[1], Julia Uitz[1], Annick Bricaud[1], Emanuele Organelli[1,2], Antoine Poteau[1], Catherine Schmechtig[3], Bernard Gentili[1], Grigor Obolensky[4], Edouard Leymarie[1], Christophe Penkerc'h[1], Fabrizio D'Ortenzio[1], and Hervé Claustre[1]

[1]Sorbonne Universités, UPMC Univ Paris 06, CNRS, Observatoire Océanologique de Villefranche, Laboratoire d'Océanographie de Villefranche, Villefranche-sur-Mer, France, [2]Plymouth Marine Laboratory, Prospect Place, The Hoe, Plymouth, United Kingdom, [3]OSU Ecce Terra, UMS 3455, CNRS and Université Pierre et Marie Curie, Paris 6, Paris, France, [4]ERIC Euro-Argo, 29280 Plouzané, France

Key Points:
- The b_{bp}-to-Chl*a* relationship varies along the water column, as well as with seasons and oceanic regions
- The b_{bp}-to-Chl*a* ratio is a valuable biogeochemical proxy for assessing the nature of the particulate assemblage and revealing photoacclimation processes
- The BGC-Argo float network yields an unprecedented amount of quality data for studying biogeochemical processes at a global scale and along the vertical dimension

Supporting Information:
- Supporting Information S1
- Supporting Information S2
- Supporting Information S3
- Table S1
- Table S2
- Table S3

Correspondence to:
M. Barbieux,
barbieux@obs-vlfr.fr

Abstract Characterizing phytoplankton distribution and dynamics in the world's open oceans requires in situ observations over a broad range of space and time scales. In addition to temperature/salinity measurements, Biogeochemical-Argo (BGC-Argo) profiling floats are capable of autonomously observing at high-frequency bio-optical properties such as the chlorophyll fluorescence, a proxy of the chlorophyll *a* concentration (Chl*a*), the particulate backscattering coefficient (b_{bp}), a proxy of the stock of particulate organic carbon, and the light available for photosynthesis. We analyzed an unprecedented BGC-Argo database of more than 8,500 multivariable profiles collected in various oceanic conditions, from subpolar waters to subtropical gyres. Our objective is to refine previously established Chl*a* versus b_{bp} relationships and gain insights into the sources of vertical, seasonal, and regional variability in this relationship. Despite some regional, seasonal and vertical variations, a general covariation occurs at a global scale. We distinguish two main contrasted situations: (1) concomitant changes in Chl*a* and b_{bp} that correspond to actual variations in phytoplankton biomass, e.g., in subpolar regimes; (2) a decoupling between the two variables attributed to photoacclimation or changes in the relative abundance of nonalgal particles, e.g., in subtropical regimes. The variability in the b_{bp}:Chl*a* ratio in the surface layer appears to be essentially influenced by the type of particles and by photoacclimation processes. The large BGC-Argo database helps identifying the spatial and temporal scales at which this ratio is predominantly driven by one or the other of these two factors.

1. Introduction

Our ability to observe the dynamics of phytoplankton biomass and associated carbon fluxes on relevant space and time scales considerably limits our understanding and prediction skills of the biogeochemical role of phytoplankton in the carbon biological pump (Honjo et al., 2014; Legendre et al., 2015; Volk & Hoffert, 1985). For example, in situ measurements of primary production and phytoplankton carbon biomass are particularly challenging and remain scarce, although novel promising techniques have been recently proposed (Graff et al., 2012, 2015; Riser & Johnson, 2008). To overcome space-time coverage sampling limitations, bio-optical oceanographers have implemented optical sensors on a variety of in situ or remote platforms, from research vessels and moorings to ocean color satellites, gliders, and profiling floats, each with specific complementary space-time observation scales (Claustre et al., 2010; Dickey, 2003). Such platforms enable to monitor bio-optical properties that serve as proxies for major biogeochemical variables. Those include the concentration of chlorophyll *a* (Chl*a*) and the particulate backscattering coefficient at 700 nm (hereafter referred simply as b_{bp}). The chlorophyll *a* concentration is the most commonly used proxy for the phytoplankton carbon biomass (Cullen, 1982; Siegel et al., 2013), although it is well known that the ratio of Chl*a* to carbon shows large fluctuations driven by a variety of factors such as phytoplankton physiology (Álvarez et al., 2016; Geider, 1993; Staehr et al., 2002) or community composition (Geider et al., 1997; Halsey & Jones, 2015; MacIntyre et al., 2002). In the absence of mineral particles (i.e., in most open ocean waters), b_{bp} generally covaries with, and is therefore used as a proxy of, the stock of particulate organic carbon (POC; Bishop, 2009; Loisel et al., 2002; Stramski et al., 1999). However, changes in the nature (composition and size) of the particle assemblage may cause large variability in the b_{bp} signal and in the POC-to-b_{bp} relationship (Bishop, 2009; Flory et al., 2004; Gardner et al., 2006; Stramski et al., 2008).

Examining bio-optical relationships, which, for example, link the inherent optical properties of particles such as absorption or scattering, to Chl*a*, has long been an area of active research in bio-optical oceanography (Bricaud et al., 1995; Huot & Antoine, 2016; Mitchell, 1992; Mitchell & Holm-Hansen, 1991; Morel et al., 2007; Organelli et al., 2017a; Smith & Baker, 1978a; Szeto et al., 2011). Among different types of applications, bio-optical relationships enable deriving biogeochemical information over a broad range of space and time scales from in situ or remote optical measurements (Huot et al., 2007; Loisel et al., 2002; Siegel et al., 2005). Such relationships are also used in semianalytical inverse models to interpret remote sensing ocean color data (Gordon et al., 1988; Loisel & Morel, 1998; Morel & Maritorena, 2001). Various studies focused on the relationship between Chl*a* and b_{bp} using data from ocean color remote sensing (Reynolds et al., 2001; Stramska et al., 2003), field cruises (Dall'Olmo et al., 2009; Huot et al., 2008), fixed mooring (Antoine et al., 2011), or Biogeochemical-Argo (BGC-Argo) profiling floats (Xing et al., 2014). All of these studies confirmed the principle of the "bio-optical assumption" (Siegel et al., 2005; Smith & Baker, 1978b), suggesting that in open ocean waters the optical properties of a water mass covary to a first order with Chl*a*. Yet depending on the considered data set, previous studies also indicate large second-order variability around the mean b_{bp} versus Chl*a* power law relationship (Brown et al., 2008; Huot et al., 2008; Xing et al., 2014). Restricted to a given period of time, region, or trophic regime and mainly to the surface layer of the water column, these studies did not lead to a thorough characterization of the variability in the relationship between Chl*a* and b_{bp} over the full range of environments encountered in the open ocean. In addition, these studies involved different methodologies for b_{bp} measurements or retrievals, so that it is difficult to untangle regional and/or seasonal variability from possible methodological biases (Sullivan et al., 2013).

The recently launched network of BGC-Argo profiling floats is progressively transforming our capability to observe optical properties and biogeochemical processes in the oceans (Biogeochemical-Argo Planning Group, 2016; Claustre et al., 2010; IOCCG, 2011; Johnson & Claustre, 2016). The current BGC-Argo bio-optical database has drastically increased over recent years and now encompasses observations collected in a broad range of hydrological, trophic, and bio-optical conditions encountered in the world's open oceans (Organelli et al., 2017a, 2017b). Based on homogeneous measurements and processing methodologies, this database offers a unique opportunity to comprehensively reassess bio-optical relationships. Based on the analysis of more than 8,500 multivariable profiles collected within the water column (0–1,000 m) by BGC-Argo floats, this study aims to (i) investigate the natural variability around the mean statistical b_{bp}-to-Chl*a* relationship at the vertical, regional, and seasonal scales and (ii) identify the underlying sources of variability.

2. Data and Methods

2.1. BGC-Argo Profiling Floats

2.1.1. BGC-Argo Database

An array of 105 BGC-Argo profiling floats was deployed in several areas of the world's oceans in the frame of several research programs (Organelli et al., 2016a, 2017a). BGC-Argo profiling float real-time data are accessible online (at ftp://ftp.ifremer.fr/ifremer/argo/dac/coriolis/), distributed as netCDF data files (Wong et al., 2013), and updated daily with new profiles. The quality-controlled database of bio-optical vertical profiles that supports this work is publicly available from SEANOE (SEA scieNtific Open data Edition) publisher (Barbieux et al., 2017). In this database, profiles of b_{bp} were eliminated when bathymetry was shallower than 400 m and a signature of b_{bp} at depth was noticeable. This allowed us to remove the data collected in waters where a coastal influence was suspected, Black Sea excepted. Hence, 8908 BGC-Argo multiparameter profiles or "stations" (corresponding to 91 different BGC-floats) collected between 8 November 2012 and 5 January 2016 were used in this study. These stations were grouped into 24 geographic areas (Table 1), following the bioregions presented in Organelli et al. (2017a), except for the Eastern Subtropical Atlantic Gyre that is missing in our database because of suspicious backscattering data from the two profiling floats deployed in this bioregion.

Our database includes measurements from a wide range of oceanic conditions, from subpolar to tropical waters and from eutrophic to oligotrophic conditions (Figure 1). For the purpose of simplifying the

Table 1
Bioregions With the Corresponding Abbreviation, Regime, and Number of Available Floats and Profiles Represented in the BGC-Argo Database Used in the Present Study.

Location	Region abbreviation	Regime	N° profiles	N° floats
Norwegian Sea	NOR_ARC	North Subpolar Gyre (NSPG)	139	1
Icelandic Basin	ICB_NASPG		828	8
Irminger Sea	IRM_NASPG		623	11
Labrador Sea	LAS_NASPG		1160	16
South Labrador Sea	SLAS_NASPG		62	2
North Atlantic Transition Zone to northern border of the Subtropical Gyre	STZ_NASPG		146	1
Atlantic to Indian Southern Ocean	ATOI_SO	Southern Ocean (SO)	910	10
Indian Sector of the Southern Ocean	IND_SO		653	6
Atlantic Sector of the Southern Ocean	ATL_SO		49	1
Ligurian Sea and Gulf of Lions	NW_MED	Mediterranean Sea (MED)	698	8
Provencal and Algero-Provencal Basin	SW_MED		417	4
Tyrrhenian Sea	TYR_MED		325	5
Ionian Sea	ION_MED		499	6
Levantine Sea	LEV_MED		511	7
Red Sea	RED_SEA	Subtropical Gyre (STG)	75	2
North Atlantic Western Subtropical Gyre	WNASTG		12	2
South Atlantic South Subtropical Gyre	SSASTG		108	1
North Atlantic Subtropical Gyre	NASTG		363	4
South Pacific Subtropical Gyre	SPSTG		281	3
New Caledonia sector of the Pacific	NC_PAC		139	2
South Atlantic Subtropical Gyre	SASTG		368	2
South Atlantic Subtropical Transition Zone	SASTZ		214	2
North Atlantic Transition Zone to Subtropical Equatorial Atlantic	EQNASTZ		187	2
Black Sea	BLACK_SEA		141	2
TOTAL			8767	106

presentation of the results, we grouped the different bioregions into five main regimes: (1) the North Atlantic Subpolar Gyre (NSPG) divided in Icelandic Basin, Labrador and Irminger Seas; (2) the Southern Ocean (SO) essentially comprising the Indian and the Atlantic sectors; (3) the Mediterranean Sea (MED) that comprises the Northwestern Basin (NW_MED), the Southwestern Basin (SW_MED), the Tyrrhenian Sea (TYR_MED), the Ionian Sea (ION_MED), and the Levantine Sea (LEV_MED); (4) the subtropical regimes (STG) that include subtropical oligotrophic waters from the North and South Atlantic and Pacific Oceans and Red Sea (RED_SEA); and (5) the Black Sea (Table 1).

2.1.2. Biogeochemical-Argo Sensor Characteristics and Sampling Strategy

The "PROVOR CTS-4" (NKE Marine Electronics Inc., France) is a profiling autonomous platform specifically designed in the context of the Remotely Sensed Biogeochemical Cycles in the Ocean (remOcean) and Novel Argo Ocean Observing System (NAOS) projects. The PROVOR CTS-4 profiling floats used in this study were equipped with a SBE 41 CTD (Seabird Inc., USA), an OCR-504 (SAtlantic Inc., USA) multispectral radiometer measuring the Photosynthetically Available Radiation over the 400–700 nm range (PAR), and an ECO3 (Combined Three Channel Sensors; WET Labs, Inc., USA) measuring the fluorescence of chlorophyll *a* and Colored Dissolved Organic Matter (CDOM) at excitation/emission wavelengths of 470/695 and 370/460 nm respectively, and the angular scattering coefficient of particles ($\beta(\theta, \lambda)$) measured at 700 nm and an angle of 124°. Measurements were collected during upward casts programmed every 1, 2, 3, 5, or 10 days depending on the mission and scientific objectives. All casts started from the parking depth at 1,000 m at a time that was sufficient for surfacing around local noon. Vertical resolution of acquisition was 10 m between 1,000 and 250 m, 1 m between 250 and 10 m, and 0.2 m between 10 m and the surface. Raw data (electronic counts) were transmitted to land, each time the floats surfaced, through Iridium two-way communication, and were converted into desired quantities. Each variable was quality-controlled according to procedures described hereafter and specifically developed for BGC-Argo data (Organelli et al., 2016b; Schmechtig et al.,

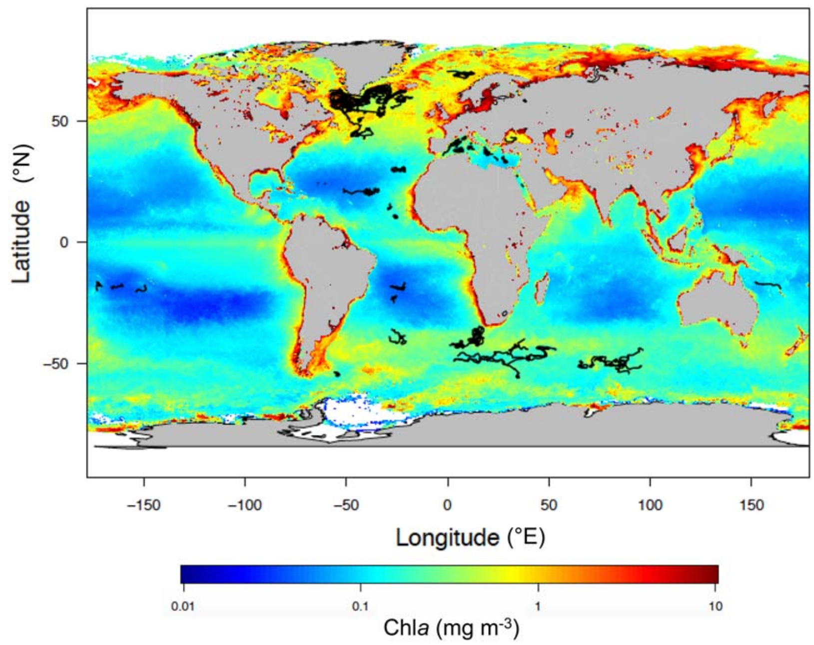

Figure 1. Geographical location of the multivariable vertical profiles collected by the BGC-Argo profiling floats represented in the database used in this study. The geographic locations are superimposed on an annual climatology of the surface chlorophyll *a* concentration derived from MODIS-Aqua climatological observations for the year 2015 (https://oceancolor.gsfc.nasa.gov/cgi/l3).

2014, 2016). Additionally, all the casts were checked for data degradation due to biofouling or instrumental drift.

2.2. Bio-Optical Data Processing

2.2.1. Chlorophyll *a* Concentration

After dark counts have been subtracted from the raw signal, chlorophyll *a* fluorescence was first converted into chlorophyll *a* concentration according to calibration coefficients provided by the manufacturer (WET Labs, 2016). Following the procedures described in Schmechtig et al. (2014), the real-time dedicated quality control procedure identified the occurrence of negative spikes, adjusted chlorophyll *a* concentration profiles for cases of nonzero values at depth and verified the range of measured values according to technical specifications provided by the manufacturer (WET Labs, 2016). In order to correct for the effect of the so-called nonphotochemical quenching (NPQ; decrease in the fluorescence-to-Chl *a* ratio under high light conditions; Kiefer et al., 1973), we systematically applied the procedure developed by Xing et al. (2012). Besides, in some bioregions such as subtropical gyres or the Black Sea, the chlorophyll *a* concentration appeared to increase at depth where it should be null. Proctor and Roesler (2010) assigned this behavior to the influence of fluorescence originating from nonalgal matter. Profiles were thus corrected according to Xing et al. (2016). Finally, following the recommendation by Roesler et al. (2017) for Chl*a* measurements from WET Labs ECO fluorometers, the calibrated quality-controlled Chl*a* values were divided by a correction factor of 2. The correction factor was deducted from a global comparison of paired HPLC (high-performance liquid chromatography) and in situ fluorescence Chl*a* data and confirmed by optical proxies of Chl*a* such as light absorption line height (Roesler & Barnard, 2013) or in situ radiometry (Xing et al., 2011). The regional variability of this average correction factor along with its possible uncertainties is fully discussed in Roesler et al. (2017). We performed a sensitivity analysis of the b_{bp}-to-Chl*a* relationship to the factor used for correcting the fluorescence-based Chl*a* values. We tested the influence of using two sets of regional factors proposed by Roesler et al. (2017) derived either from HPLC analyses or radiometric measurements, compared to the global factor of 2. Except for the Southern Ocean that appears more sensitive than other regions to the choice of the correction factor, our analysis reveals that the regional factors induce minor changes to the b_{bp}-to-Chl*a* relationship. Overall, those minor changes have little impact on the interpretation of our results. Thereafter our analysis considers Chl*a* values originating from the global correction factor. Details of the sensitivity analysis may be found in electronic supporting information A.

2.2.2. Particulate Backscattering Coefficient

We followed the procedure established by Schmechtig et al. (2016). Backscattering sensors implemented on floats provide the angular scattering coefficient β at 124° and at 700 nm. The particulate backscattering coefficient was calculated following Boss and Pegau (2001):

$$b_{bp}(700)\ (m^{-1}) = \chi(124) \times 2\pi \times \{\beta(124,700) - \beta_{sw}(124,700)\} \quad (1)$$

with $\beta(124{,}700)\ (m^{-1}\ sr^{-1}) = \text{slope} \times (\text{counts} - b_b\text{dark})$

where the (instrument-specific) slope and $b_b$dark are provided by the manufacturer, and $\chi(124)$ is equal to 1.076 (Sullivan et al., 2013). The contribution of pure seawater (β_{sw}) was removed and computed according to Zhang et al. (2009). Finally, vertical profiles were quality-controlled by verifying the range of measured values according to the technical specifications provided by the manufacturer (WET Labs, 2016) and removing negative spikes following Briggs et al. (2011). Remaining spikes were removed by applying a median filter (five-point window).

2.2.3. Estimation of Uncertainty in the b_{bp}-to-Chl*a* Ratio

The backscattering and chlorophyll fluorescence sensors implemented on floats are all ECO3 sensors (WET Labs, Inc.). This avoids heterogeneous sources of uncertainties associated with various sensors (see e.g., Roesler et al., 2017). In addition, the data are calibrated and qualified following the recommended standard BGC-Argo procedure presented in Schmechtig et al. (2016). A thorough estimation of the uncertainties affecting the different parameters would necessitate an entirely dedicated study, which is beyond the scope of the present one. However, an estimation of the average error that may influence our results has been made.

Accounting for measurement error only, we assume an error $\sigma\, b_{bp}(700)(m^{-1}) = 2.2 \times 10^{-6}$ for the b_{bp} sensor and $\sigma\,\mathrm{Chl}\ a\,(mg\ m^{-3}) = 0.007$ for the chlorophyll fluorescence sensor, as provided by the manufacturer. Following an error propagation law (Birge, 1939; Ku, 1966), the combined effect of these errors on the b_{bp}-to-Chl*a* ratio can be computed and a relative error (in %) can be obtained as

$$\sigma\left[b_{bp}/\mathrm{Chl}a\right] = \sqrt{\frac{\frac{\sigma {b_{bp}}^2}{\mathrm{Chl}a^2} + \frac{{b_{bp}}^2 \times \sigma\mathrm{Chl}a^2}{\mathrm{Chl}a^4} - \frac{2 \times b_{bp} \times \mathrm{cor}\left(b_{bp},\mathrm{Chl}a\right) \times \sigma b_{bp} \times \sigma\mathrm{Chl}a}{\mathrm{Chl}a^3} \times \mathrm{Chl}a}{b_{bp}}} \quad (2)$$

With cor (b_{bp}, Chl*a*) corresponding to the correlation between the particulate backscattering coefficient and the chlorophyll *a*. Considering the surface data, a median error of 0.11% is obtained and 80% of the data show relative errors lower than 10% (Figure 2a). Relative errors larger than 10% appear for the lowest values of b_{bp} ($<10^{-3}\ m^{-1}$) and Chl*a* ($<10^{-2}\ mg\ m^{-3}$; Figure 2b), which corresponds to the clearest waters of the oligotrophic gyres. In addition, a sensitivity analysis described in supporting information A indicates that correcting the fluorescence-based Chl*a* values of the database with regional factors compared to a global factor does not significantly affect the distribution of the computed errors in the b_{bp}-to-Chl*a* ratio.

2.3. Derived Variables

2.3.1. Physical and Biogeochemical Layers of the Water Column

We consider four different layers of the water column: (i) the productive layer (Morel & Berthon, 1989) comprised between the surface and 1.5 Z_{eu}, with Z_{eu} corresponding to the euphotic depth which is the depth at which PAR is reduced to 1% of its surface value; (ii) the mixed layer where all properties are expected to be homogenous and that encompasses a large fraction of the phytoplankton biomass (Brainerd & Gregg, 1995; Taylor & Ferrari, 2010); (iii) the surface layer, observable by satellite remote sensing, extending from surface to the first optical depth (Z_{pd}; Gordon & McCluney, 1975); and (iv) the deep chlorophyll maximum (DCM) layer (i.e., thickness of the DCM) where different processes may lead to a Chl*a* enhancement. Unlike the productive layer, the surface, the mixed and the deep chlorophyll maximum layers are considered as homogeneous layers where the phytoplankton population is expected to be acclimated to the same light and nutrient regimes. The 0–1.5Z_{eu} layer is chosen to estimate the average b_{bp}-to-Chl*a* ratio in the entire enlightened layer of the water column, even if it is acknowledged that large variations in this ratio may occur throughout this layer. This average b_{bp}-to-Chl*a* ratio is thereafter used as a reference to which we compare the ratios calculated for the other layers of the water column.

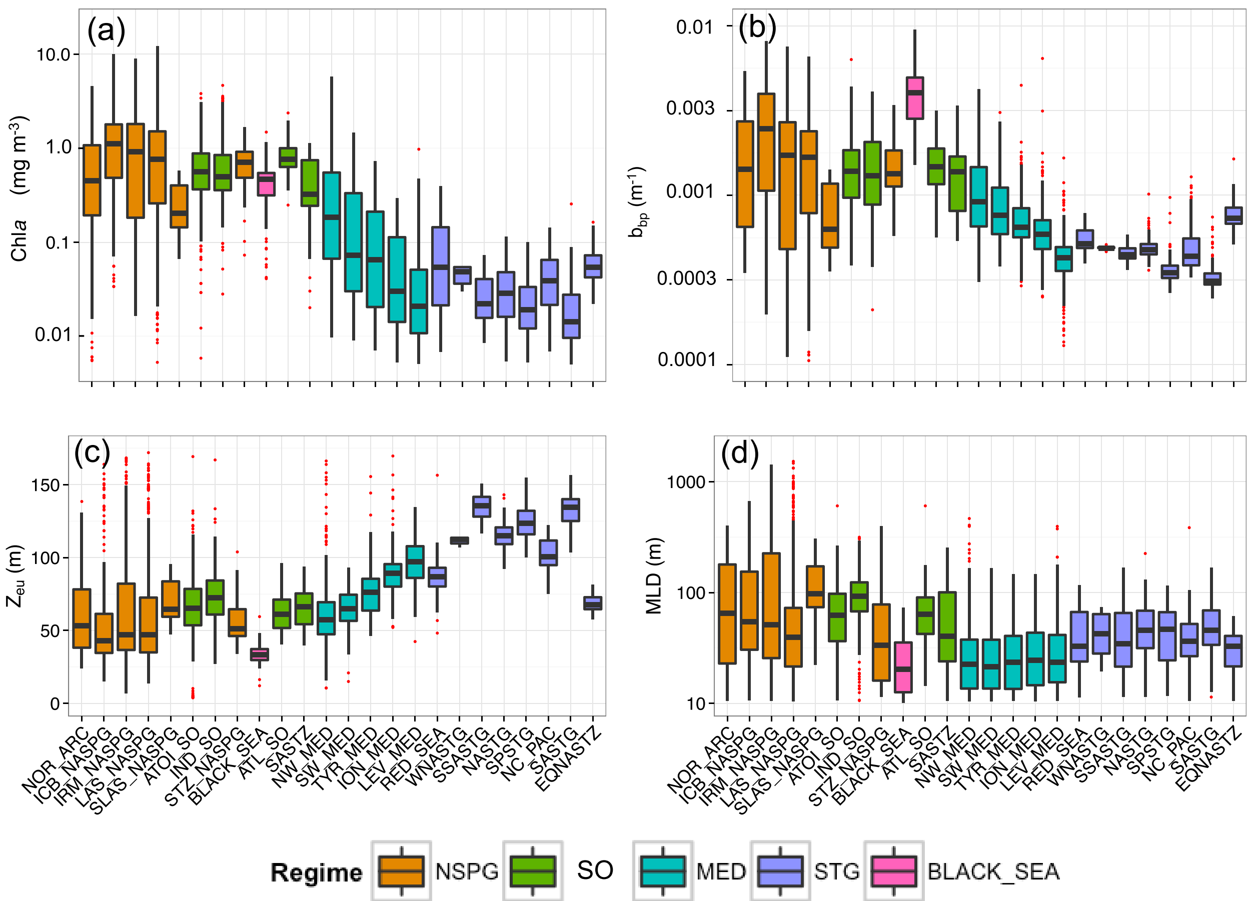

Figure 2. Boxplot of the distribution, for each of the 24 bioregions represented in the BGC-Argo database used in this study, of the (a) chlorophyll *a* concentration (Chl*a*) in the surface (0-Z_{pd}) layer, (b) particulate backscattering coefficient at 700 nm (b_{bp}) in the surface (0-Z_{pd}) layer, (c) depth of the euphotic layer (Z_{eu}), and (d) mixed layer depth (MLD). Note that the bioregions are ordered following the absolute value of the latitude and, within the Mediterranean Sea, following the longitude (i.e., from west to east). Red points beyond the end of the whiskers represent outliers beyond the 1.5 × IQR (IQR = interquartile range) threshold.

The mixed layer depth (MLD) was determined using a 0.03 kg m^{-3} density criterion (de Boyer Montégut, 2004). The euphotic depth Z_{eu} and the penetration depth, $Z_{pd} = Z_{eu}/4.6$, were computed from the BGC-Argo PAR vertical profiles following the procedure described in Organelli et al. (2016b). Values of Z_{eu} and Z_{pd} are available from Organelli et al. (2016a). To study more specifically the dynamics of the bio-optical properties in the DCM layer and because the width of a DCM may fluctuate in space and time, we adjusted a Gaussian profile to each vertical profile of Chl*a* of the database that presented a deep Chl*a* maximum and computed the width of this DCM. This parameterizing approach proposed by Lewis et al. (1983) has been widely used to fit vertical profiles of Chl*a* (e.g., Morel & Berthon, 1989; Uitz et al., 2006) such as

$$c(z) = c_{max} e^{-\left(\left(\frac{z - z_{max}}{\Delta z}\right)^2\right)} \quad (3)$$

where c(z) is the Chl*a* concentration at depth z, c_{max} is the Chl*a* concentration at the depth of the DCM (z_{max}), and Δz, the unknown, is the width of the DCM.

In order to retrieve Δz, the unknown parameter, we performed an optimization of equation (3) with a maximum width set at 50 m so only the profiles with a relatively pronounced DCM are kept. Then we computed the mean Chl*a* and b_{bp} for the layer that represents the thickness of the DCM.

Finally, all quality-controlled profiles of Chl*a* and particulate backscattering coefficient were averaged within the different considered layers.

2.3.2. Environmental and Biological Parameters

In order to analyze the variability in the b_{bp}-to-Chl*a* relationship, we consider the role of the light conditions in the various layers of the water column, i.e., the productive, mixed, surface, and DCM layers. The vertical profiles of b_{bp}:Chl*a* and PAR were averaged within each of the four considered layers. For each layer and both variables, the median value was computed monthly and regionally (i.e., for each regime). For each layer and each regime, we determined the maximum observed PAR that was used to normalize the monthly median PAR values of the corresponding layer and regime (PAR_{norm}). Ultimately, for each layer and each regime, the monthly median PAR_{norm} values were classified into four different intervals (0–0.25; 0.25–0.50; 0.50–0.75; 0.75–1), and the monthly averaged b_{bp}: Chl*a* values were assigned to one of these four PAR_{norm} intervals.

Using the method of Uitz et al. (2006), an index of the phytoplankton community composition, based on the relative contributions of size classes to total chlorophyll *a*, was also computed from the surface Chl*a* values. We applied this procedure to the surface Chl*a* values from our BGC-Argo database that we further monthly averaged to finally obtain the relative contributions of microphytoplankton to the total chlorophyll *a* biomass for each bioregion within the 0-Z_{pd} layer.

3. Results

3.1. Overview of the BGC-Argo Database

A latitudinal decreasing gradient of surface Chl*a* is observed from the North Subpolar Gyre (NSPG) and Southern Ocean (SO) regimes to the subtropical (STG) regime with a median Chl*a* from $\sim$1 mg m^{-3} to $\sim$0.05 mg m^{-3}, respectively (Figure 2a). It is noteworthy that, in our data set where the South East Pacific Ocean is not represented, the South Atlantic Subtropical Gyre (SASTG) is the most oligotrophic bioregion, experiencing the lowest median Chl*a* (0.014 mg m^{-3}) and the highest median Z_{eu} (135 m). A west-to-east trophic gradient is observed in the Mediterranean Sea, with median surface Chl*a* values of 0.186 and 0.025 mg m^{-3} in the Northwestern Basin and the Levantine Sea, respectively (Figure 2a).

A similar pattern is observed in the surface particulate backscattering coefficient values (Figure 2b). Median surface b_{bp} values range between $\sim$0.002 m^{-1} in NSPG and $\sim$0.0003 m^{-1} in STG regime. In the Mediterranean Sea, the b_{bp} values vary over 1 order of magnitude, with maximum values found in the Northwestern Basin and minimum values in the Levantine Sea. The North Atlantic Transition Zone to Subtropical Equatorial Atlantic (EQNASTZ) bioregion exhibits particularly high values of b_{bp} compared to other STG regions (Figure 2a). The Z_{eu} values also show a latitudinal gradient (Figure 2c), with median values of $\sim$50 m in NSPG and $\sim$125 m in STG regimes. The median MLD shows a significant variability among the 24 bioregions (Figure 2d). The distribution of the MLD in the Mediterranean Sea is centered on a low median value of 23 m, but very large values ($>$250 m) are episodically observed in the Northwestern Mediterranean (NW_MED). The deepest mixed layers (median value of 98 m) are observed in the South Labrador Sea (SLAS_NASPG), and episodes of extremely deep mixed layers ($\sim$1,000 m) are also recorded in the Labrador Sea (LAS_NASPG). The shallowest mixed layers are observed in the Black Sea ($\sim$20 m). It is also worth to notice that MLD values in STG are particularly stable and feature very few outliers.

3.2. Variability in the b_{bp}-to-Chl*a* Relationship at the Global Scale Within Distinct Layers of the Water Column

3.2.1. The Productive Layer

In this layer, the b_{bp}-to-Chl*a* relationship follows a power law ($R^2 = 0.74$; Figure 3a). Yet when data from different regimes and bioregions are considered separately, regional and seasonal patterns emerge. Bioregions of the subpolar NSPG and SO regimes (Figures 4a–4i) show a significant correlation between Chl*a* and b_{bp} with high R^2 ($>$0.60) and slope (i.e., exponent of the power law) always above 0.50 (except for the Norwegian Sea, Figure 4a). Minimal values of both Chl*a* and b_{bp} are encountered in winter whereas maximal values are reached in summer. Deviations from the global log-log linear model occur in some bioregions of the NSPG regime, e.g., in the Icelandic Basin (ICB_NASPG) in summer (Figure 4b) and are characterized by an abnormally high b_{bp} signal considering the observed Chl*a* levels. Such a deviation is found all year long in the Black Sea, where a correlation between Chl*a* and b_{bp} is no longer observable ($R^2 = 0.09$; Figure 4x).

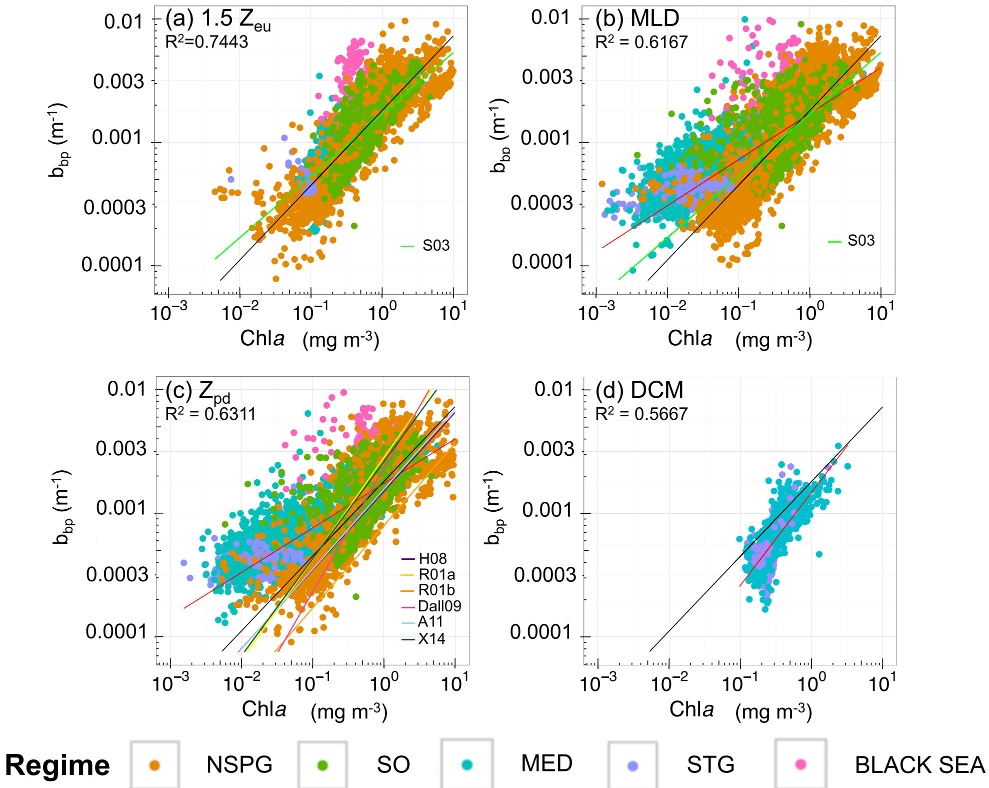

Figure 3. Log-log scatterplot of the particulate backscattering coefficient at 700 nm (b_{bp}) as a function of the chlorophyll *a* concentration (Chl*a*) within (a) the productive layer comprised between the surface and $1.5Z_{eu}$, (b) the mixed layer, (c) the surface (0-Z_{pd}) layer, and (d) at the level of the deep chlorophyll maximum (DCM). The color code indicates the regime where the Biogeochemical-Argo data were collected. For each plot, the black line represents the relationship calculated over the productive layer (0–$1.5Z_{eu}$) while the red line corresponds to the regression model calculated over the considered layer. The other lines represent regression relationships from the literature summarized in Table 2.

In the Mediterranean Sea, the slope and R^2 decrease from the Northwestern Basin (NW_MED, Figure 4j) to the Levantine Sea (LEV_MED, Figure 4n), where Chl*a* appears to be decoupled from b_{bp}. In the Mediterranean Sea, a seasonal pattern is noticeable principally in the NW_MED, where the highest values of Chl*a* and b_{bp} are found in spring. Except for the South Atlantic Subtropical Transition Zone (SASTZ) that displays a steep slope and a high R^2 value (0.68 and 0.80, respectively), regions from the subtropical regime do not show any significant correlation between Chl*a* and b_{bp}, featuring the lowest slope and R^2 values of the b_{bp}-to-Chl*a* relationship (Figures 4o–4w). This clearly suggests a decoupling between those two properties. In these oligotrophic environments, different production regimes are delineated along the vertical axis in the upper and lower part of the euphotic zone. One may expect that the b_{bp}-to-Chl*a* relationship will vary depending on the considered layer. In this perspective, we further investigate the behavior of the bio-optical properties in different layers of the water column, namely the mixed layer, the surface layer, and the DCM layer.

3.2.2. The Mixed and Surface Layers

The distribution of Chl*a* and b_{bp} data for the surface and mixed layers shows similar patterns (Figures 3b and 3c). The distribution in the surface layer shows two distinct trends. With the exception of the Atlantic to Indian Southern Ocean (ATOI_SO) bioregion that shows an important dispersion of b_{bp} values during summer, the data collected in the NSPG and SO regimes and NW_MED bioregions exhibit a clear log-log linear covariation between Chl*a* and b_{bp} associated with slopes above 0.3 and high R^2 (Figures 5a–5j), similarly to what is observed for the productive layer (Figures 3a and 4). In the subpolar NSPG and SO regimes, values of b_{bp} and Chl*a* in the 0-Z_{pd} layer reach their maximal values in summer (Figures 5a–5i), whereas in the NW_MED, the highest values are recorded in spring (Figure 5j). Data from the subtropical regime (STG) form a separate cluster where Chl*a* and b_{bp} are decoupled, with generally very low R^2 values. Chl*a* values

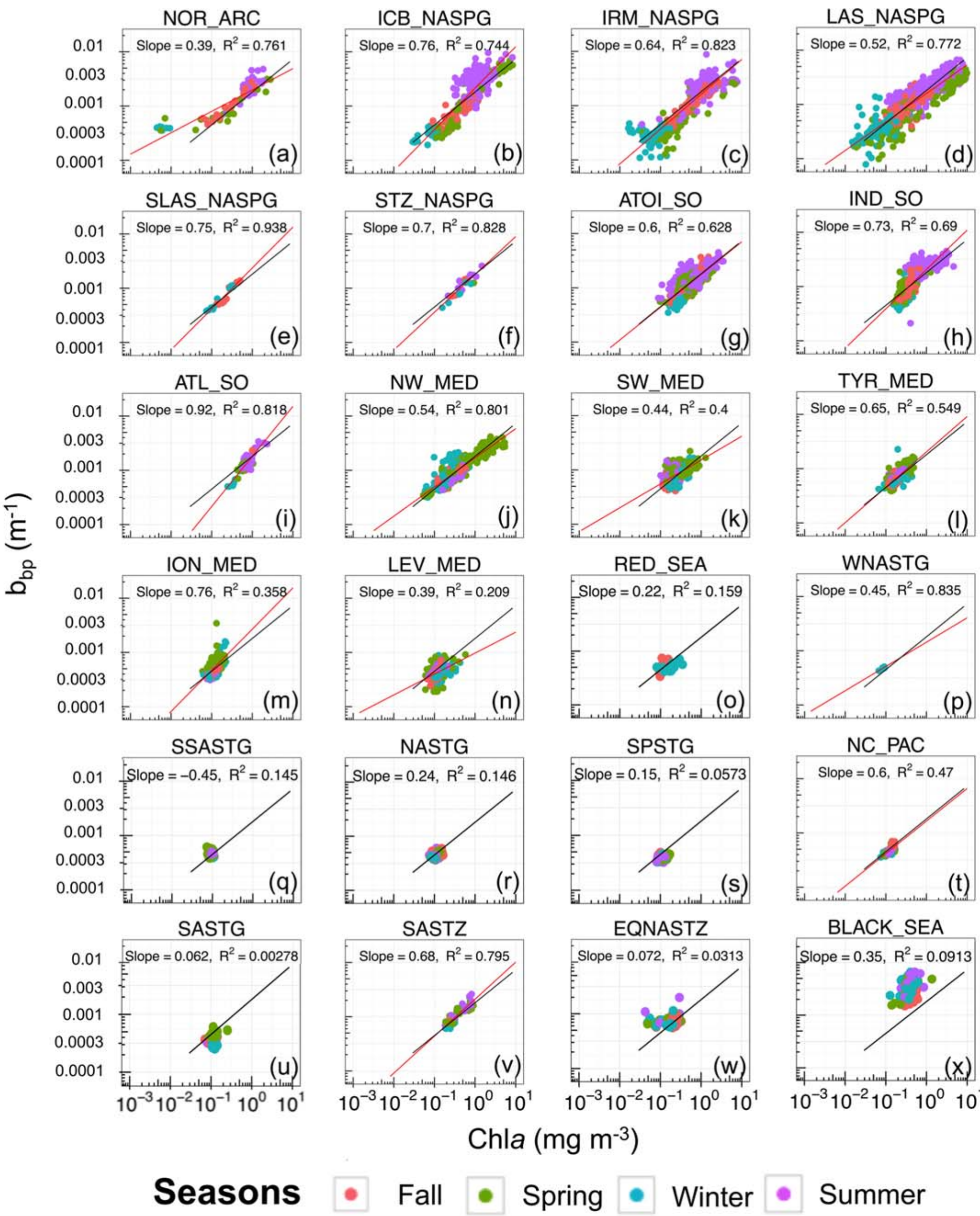

Figure 4. Log-log scatterplot of the particulate backscattering coefficient at 700 nm (b_{bp}) as a function of the chlorophyll *a* concentration (Chl*a*) within the layer comprised between the surface and $1.5Z_{eu}$ for each bioregion. The color code indicates the seasons. The black line represents the average relationship calculated in this layer considering all bioregions and the red line corresponds to the regression model calculated for each bioregion considered here (when $R^2 > 0.2$).

encountered are almost always under 0.1 mg m^{-3} and the slope of the relationship remains under 0.2. Whereas b_{bp} values remain constant all over the seasons, a seasonal increase of Chl*a* is observable with noticeable higher winter values (Figures 5o–5w).

The MED Sea is characterized by a gradual decrease in the Chl*a* and b_{bp} covariation across a longitudinal trophic gradient (Figures 5j–5n) from the NW_MED (slope = 0.33, $R^2 = 0.66$) to the LEV_MED (slope = 0.15, $R^2 = 0.21$). The Eastern Mediterranean basin does not feature any spring maximum in Chl*a* and b_{bp} (Figures 5m and 5n). However, there is a noticeable winter increase in Chl*a* as reported also in the STG regime. Regarding the Black Sea bioregion, high values of both variables are observed and no seasonal pattern is noticed (Figure 5x), consistent with what is observed in the productive layer.

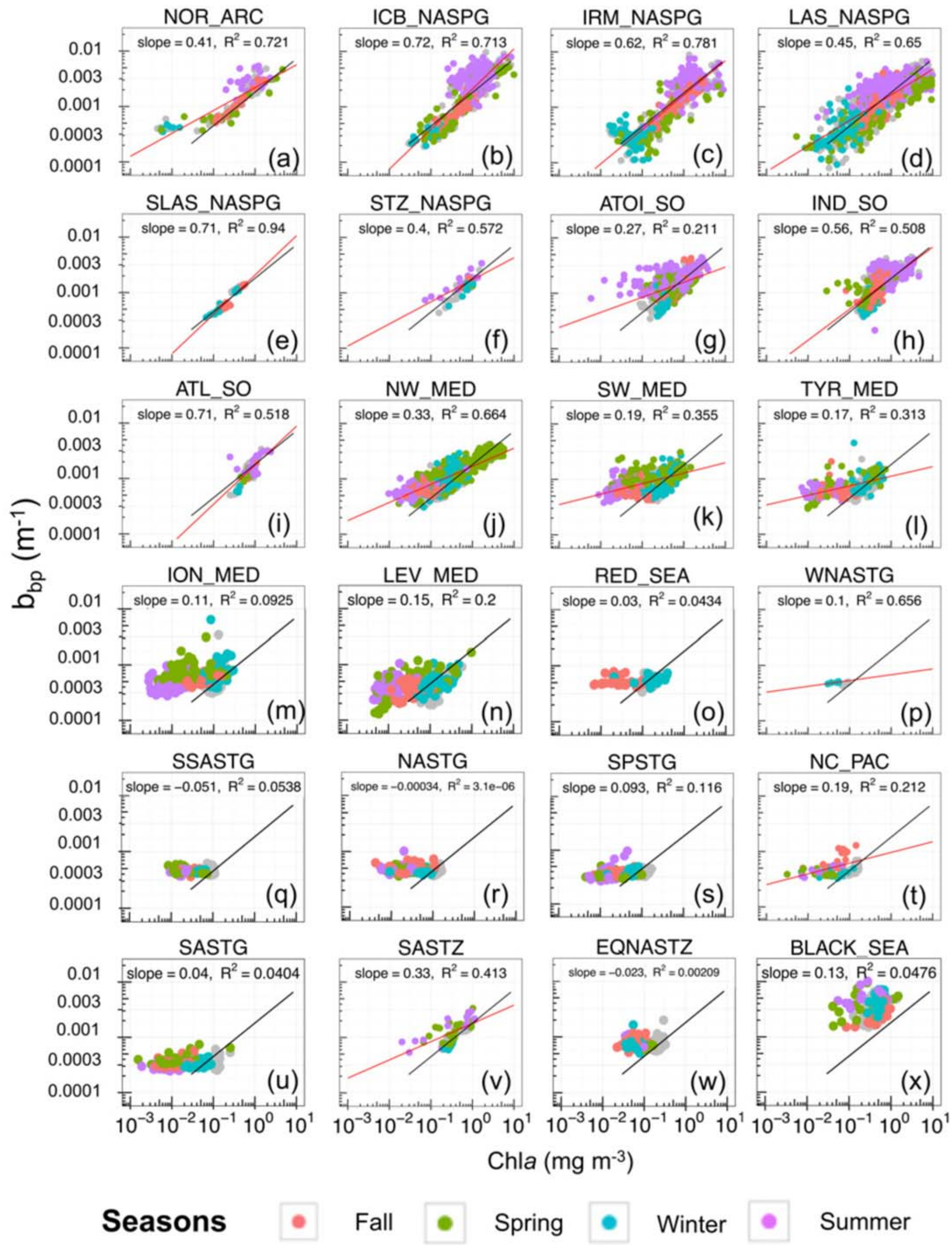

Figure 5. Log-log scatterplot of the particulate backscattering coefficient at 700 nm (b_{bp}) as a function of the chlorophyll *a* concentration (Chl*a*) within the surface layer (0-Z_{pd}) for each bioregion. The color code indicates the seasons. For each plot, the black line represents the average relationship calculated for the surface layer (0-Z_{pd}) for the entire database while the red line is the regression model calculated for each bioregion (shown only if $R^2 > 0.2$). The data points for the productive layer are shown in grey color.

3.2.3. The Deep Chlorophyll Maximum Layer

The analysis of the b_{bp}-to-Chl*a* relationship at the level of the DCM obviously considers only the seasonal or permanent stratified regimes (and bioregions) where a DCM occurs, i.e., the Mediterranean and subtropical regimes. The b_{bp}-to-Chl*a* relationship in the DCM layer gradually deviates from the relationship established in the productive layer considering all bioregions (Figure 3d). Chl*a* is systematically higher by a factor ∼2 regardless of the bioregion and never reaches values below 0.1 mg m^{-3} (Figures 3d and B1 in electronic supporting information B).

The subset of data from this layer also shows two distinct trends in the b_{bp}-to-Chl*a* relationship, for Chl*a* values below or above 0.3 mg m^{-3} (Figure 3d). For Chl*a* > 0.3 mg m^{-3}, a positive correlation between b_{bp} and Chl*a* can be noticed, although with a large dispersion of the data around the regression line, whereas for Chl*a* < 0.3 mg m^{-3}, Chl*a* and b_{bp} exhibit a strong decoupling. The MED Sea (Figures B1a–B1e in electronic supporting information B) is characterized by a stronger covariation between Chl*a* and b_{bp} than the STG regime (Figures B1f–B1n in electronic supporting information B) ($R^2 = 0.53$ for NW_MED versus $R^2 = 0.10$ for SPSTG). In the Mediterranean Sea, DCMs are seasonal phenomena occurring essentially in summer or fall (e.g., Siokou-Frangou et al., 2010). A covariation between b_{bp} and Chl*a* occurs as soon as a DCM takes place, with maximum values of b_{bp} and Chl*a* encountered in summer when the DCM is the most pronounced, in both the western and eastern Mediterranean basins. On the opposite, in the STG regime where durable stratification takes place, DCMs appear as a permanent pattern. The b_{bp} and Chl*a* variations are decoupled and the highest values of both variables are recorded in spring or fall.

4. Discussion

The present analysis of a global BGC-Argo database indicates a general power relationship between b_{bp} and Chl*a* in the productive layer as well as in the surface and mixed layers. Nevertheless, the analysis of subsets of data suggests a large second-order variability around the global mean relationships, depending on the considered range of values in Chl*a* and b_{bp}, layer of the water column, region, or season. In this section, we investigate the sources of variability around the average b_{bp}-to-Chl*a* relationship in our database.

4.1. General Relationship Between Chl*a* and b_{bp}

The chlorophyll *a* concentration is the most commonly used proxy for the phytoplankton carbon biomass (Cullen, 1982; Siegel et al., 2013), whereas the particulate backscattering coefficient is considered as a proxy of the POC in open ocean (Balch et al., 2001; Cetinić et al., 2012; Dall'Olmo & Mork, 2014; Stramski et al., 1999) and provides information on the whole pool of particles, not specifically on phototrophic organisms. Over broad biomass gradients, the stock of POC covaries with phytoplankton biomass and hence b_{bp} and Chl*a* show substantial covariation. This is what is observed in the present study when the full database is considered (Figure 3a). This is also the case when we examine subsets of data from the NSPG and SO regimes that feature strong seasonality and show relatively constant relationships between b_{bp} and Chl*a* (Figures 3a–3c, 4a–4l, and 5a–5i). In such environments, an increase in the concentration of chlorophyll *a* is associated with an increase in b_{bp}. Such significant relationships between b_{bp} and Chl*a* have indeed been reported in several studies based on relatively large data sets (Huot et al., 2008) or measurements from seasonally dynamic systems (Antoine et al., 2011; Stramska et al., 2003; Xing et al., 2014). Our results corroborate these studies and yield a global relationship of the form $b_{bp}(700) = 0.00181\ (\pm 0.000001)\ \mathrm{Chl}a^{0.605\ (\pm 0.005)}$ for the productive layer.

Nevertheless, the b_{bp}-to-Chl*a* relationship is largely variable depending on the considered layer of the water column. Regarding the mixed and surface layers, our study suggests a general relationship with determination coefficients smaller than those calculated for the productive layer. The intercept ($\sim$0.0017) and more importantly the slope values ($\sim$0.36) associated with the surface layer are also lower than those associated with the productive layer (Table 3); hence, for a given level of b_{bp}, the Chl*a* is lower for the surface layer than predicted by the productive layer relationship. Empirical relationships of the literature previously established in various regions in the first few meters of the water column (Antoine et al., 2011; Dall'Olmo et al., 2009; Reynolds et al., 2001; Xing et al., 2014) always show steeper slope compared to our results for the surface layer (Table 2).

To our knowledge, the present study proposes the first analysis of the b_{bp}-to-Chl*a* relationship within the DCM layer. A significant relationship between b_{bp} and Chl*a* is observed and it is associated with the steepest slope, the highest RMSE and the lowest coefficient of determination in comparison with the other layers (Table 3). Thus, for the DCM layer, a given level of b_{bp} is associated with higher values of Chl*a* than predicted by the global relationship of the productive layer.

Table 2

Empirical Relationship Between the Particulate Backscattering Coefficient (b_{bp}) and the Concentration Of Chlorophyll a *(Chl* a*) Previously Published in the Literature With the Corresponding Reference and Abbreviation, Region, and Layer of the Water Column Considered for Analysis*

Empirical relationship	Region	Layer in the water column	Abbreviation	Reference
$b_{bp}(\lambda) = 0.0023 - 0.000005 (\lambda - 550)\ \mathrm{Chl}a^{0.565 + 0.000486(\lambda - 550)}$	Eastern South Pacific	$2/K_d(490)$	H08	Huot et al. (2008)
$b_{bp}(555) = 0.004\ \mathrm{Chl}a^{0.822}$	Antarctic Polar Front	15 m	R0l a	Reynolds et al. (2001)
$b_{bp}(555) = 0.001\ \mathrm{Chl}a^{0.667}$	Ross Sea	15 m	R0l b	Reynolds et al. (2001)
$b_{bp}(555) = 0.0019\ \mathrm{Chl}a^{0.61}$	Polar North Atlantic	MLD	S03	Stramska et al. (2003)
$b_{bp}(526) = 0.00386\ \mathrm{Chl}a$	Eastern Equatorial Pacific	Surface	Dall09	Dall'Olmo et al. (2009) modified in Xing et al. (2014)
$b_{bp}(532) = 0.003\ \mathrm{Chl}a^{0.786}$	North Atlantic Subpolar Gyre	Z_{pd}	X14	Xing et al. (2014)
$b_{bp}(555) = 0.00197\ \mathrm{Chl}a^{0.647}$	North-Western Mediterranean Sea and Santa Barbara Channel	Surface	All	Antoine et al. (2011)

In the next two sections, we will investigate the underlying processes leading to the existence or not of a relationship between b_{bp} and Chl*a* and explore the variability of this relationship along the vertical dimension, the seasons and the distinct bioregions of the different regimes. For this purpose, we will consider the behavior of the b_{bp}:Chl*a* ratio with respect to light conditions and phytoplankton community composition.

4.2. Influence of the Nature of the Particulate Assemblage on the b_{bp}-to-Chl*a* Relationship

Although the relationship between POC and b_{bp} is evident in some regions, the particulate backscattering coefficient is not a direct proxy of POC. It depends on several parameters such as the concentration of particles in the water column, their size distribution, shape, structure, and refractive index (Babin & Morel, 2003; Huot et al., 2007; Morel & Bricaud, 1986; Whitmire et al., 2010). The b_{bp} coefficient has been shown to be very sensitive to the presence of picophytoplankton as well as of nonalgal particles of the submicron size range (e.g., detritus, bacteria, and viruses), especially in oligotrophic waters (Ahn et al., 1992; Stramski et al., 2001; Vaillancourt et al., 2004), but also to particles up to 10 μm (Loisel et al., 2007).

In regions with substantial inputs of mineral particles, a shift toward enhanced b_{bp} values for a constant Chl*a* level occurs (Figures 4w and 4x, 5w and 5x). Substantial concentrations of mineral particles, submicrometer particles of Saharan origin, for example, have been shown to cause significant increases in the particulate backscattering signal (Claustre et al., 2002; Loisel et al., 2011; Prospero, 1996; Stramski et al., 2004). The EQNASTZ bioregion exhibits, for example, particularly high b_{bp} values compared to the low Chl*a* found in the surface layer (Figures 4w and 5w). This is not surprising considering that this region is located in the Equatorial North Atlantic dust belt (Kaufman et al., 2005). The Black Sea is also characterized by a higher b_{bp} signal than predicted from Chl*a* based on our global model (Figures 4x and 5x). This could be explained by the fact that this enclosed sea follows a coastal trophic regime and is strongly influenced by river runoff that may carry small and highly refractive lithogenic particles (Ludwig et al., 2009; Tanhua et al., 2013). Such an increase in backscattering signal may also be related to coccolithophorid blooms (Balch et al., 1996a). These small calcifying microalgae highly backscatter light due to their calcium carbonate shell and their presence could explain the episodically higher b_{bp} than predicted by the global regression model

Table 3

Empirical Relationship Obtained Between the Particulate Backscattering Coefficient (b_{bp}) and the Concentration of Chlorophyll a *(Chl* a*) for the Different Layers of the Water Column Considered in This Study*

Empirical relationship	Water column layer	R^2	RMSE	Number of data
$b_{bp}(700) = 0.00174\ \mathrm{Chl}a^{0.360}$	$0\text{-}Z_{pd}$	0.6311	0.000942	5,253
$b_{bp}(700) = 0.00171\ \mathrm{Chl}a^{0.373}$	0-MLD	0.6167	0.000932	8,743
$b_{bp}(700) = 0.00147\ \mathrm{Chl}a^{0.753}$	DCM	0.5667	0.00104	1,628
$b_{bp}(700) = 0.00181\ \mathrm{Chl}a^{0.605}$	$0-1.5Z_{eu}$	0.7443	0.000967	5,250

Note. We also indicate the associated statistics: Root-mean-squared error (RMSE) and coefficient of determination R^2 for the significance level of $p < 0.001$.

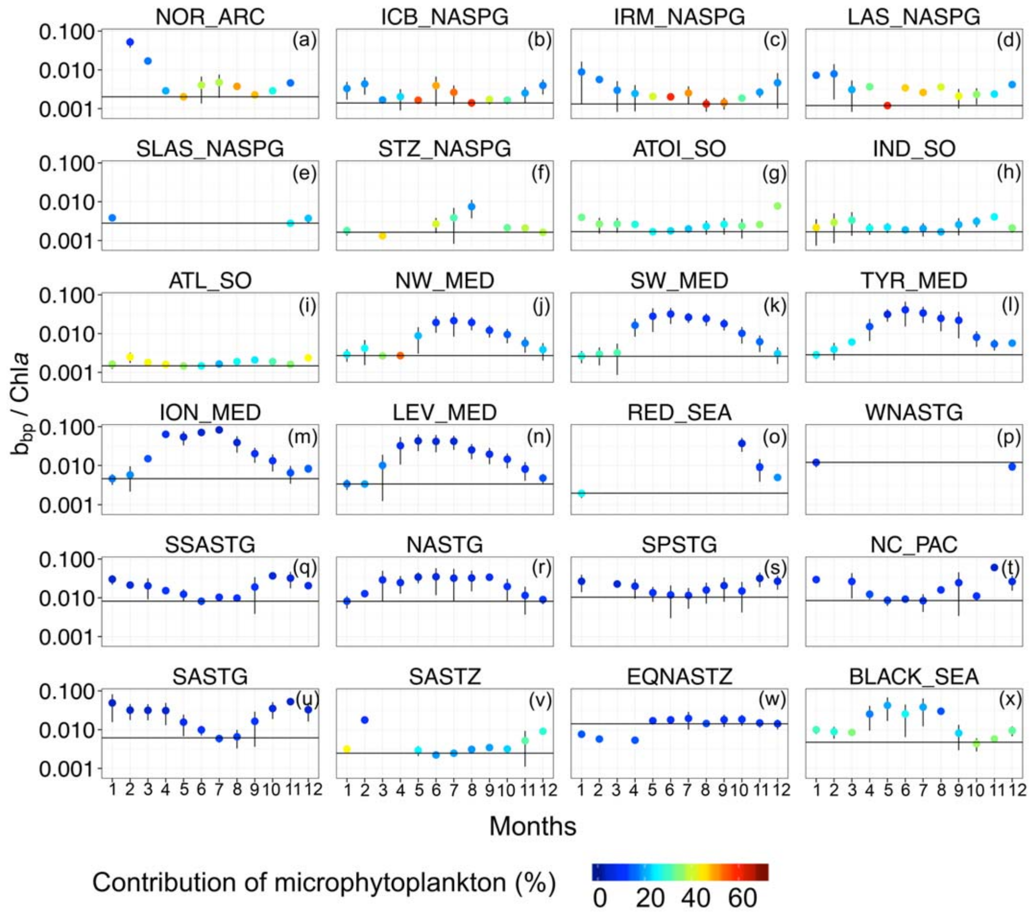

Figure 6. Monthly climatology of the b_{bp}:Chl*a* ratio within the surface layer (0-Z_{pd}). The color code indicates the fractional contribution of the microphytoplankton to the chlorophyll biomass associated with the entire phytoplankton assemblage, estimated from the Uitz et al. (2006) parameterization. In each figure, the horizontal black line shows the minimum value of the b_{bp}:Chl*a* ratio determined within each bioregion. The black lines represent the standard deviation for each data point.

particularly in the Black Sea where coccolithophorid blooms are frequently reported (Cokacar et al., 2001; Kopelevich et al., 2014) or in the Iceland Basin (Balch et al., 1996b; Holligan et al., 1993; Figure 4b or 5b).

Recently, the b_{bp}:Chl*a* ratio, proxy of the POC:Chl*a* ratio (Álvarez et al., 2016; Behrenfeld et al., 2015; Westberry et al., 2016), has been used as an optical index of phytoplankton communities, with low values associated with a dominance of diatoms in the phytoplankton assemblage (Cetinić et al., 2012, 2015). Indeed, in open ocean waters, phytoplankton generally dominate the pool of particles in the water column. A shift toward higher or weaker b_{bp} values at a constant Chl*a* level may be explained by changes in the phytoplankton community composition. However, in oligotrophic environments, nonalgal particles may represent a significant part of the particulate assemblage (Loisel et al., 2007; Stramski et al., 2004; Yentsch & Phinney, 1989). Indeed, a background of submicronic living biological cells such as viruses and bacteria or even nonliving particles including detritus or inorganic particles could influence the b_{bp}:Chl*a* ratio (e.g., Claustre et al., 1999; Morel & Ahn, 1991; Stramski et al., 2001).

The lowest b_{bp}:Chl*a* values in our global database occur in summer in the NSPG and SO regimes (Figures 6a–6i) and are associated with large contributions (>40%) of microphytoplankton to the total Chl*a*. This actually corroborates the hypothesis of Cetinić et al. (2012, 2015) that b_{bp}:Chl*a* can be considered as an optical index of the phytoplankton community composition. High values of the b_{bp}:Chl*a* ratio are associated with large contributions of picophytoplankton and nanophytoplankton to algal biomass and low values with diatom-dominated communities. The occurrence of microphytoplankton blooms of large-sized phytoplankton community is indeed well known in the NSPG regime (Barton et al., 2015; Cetinić et al., 2015; Li, 2002) or in some productive regions of the Southern Ocean (Georges et al., 2014; Mendes et al., 2015; Uitz et al., 2009). Similarly, in the NW_MED bioregion, low b_{bp}:Chl*a* values are accompanied by large contributions of microphytoplankton during the spring bloom (Marty & Chiavérini, 2010; Mayot et al., 2016; Siokou-Frangou et al., 2010). On the opposite, high b_{bp}:Chl*a* values in summer are rather associated with dominant contributions of the picophytoplankton and nanophytoplankton to the total chlorophyll biomass (Figure 6j) and also possibly to a higher proportion of nonalgal particles, consistently with Navarro et al. (2014) or Sammartino et al. (2015).

In the rest of the Mediterranean Basin (SW_MED, TYR_MED and the Eastern Basin) (Figures 6k–6n) as well as in the subtropical regime, the phytoplankton biomass is essentially constant throughout the year with high b_{bp}:Chl*a* values in summer, lower values in winter, and a relatively constant picoplankton-dominated algal community (Figures 6o–6w; Dandonneau et al., 2004; Ras et al., 2008; Uitz et al., 2006). In this region, the seasonal cycle of the b_{bp}:Chl*a* ratio does not seem to be influenced at a first order by changes in phytoplankton community composition.

4.3. Influence of Photoacclimation on the b_{bp}-to-Chl*a* Relationship

The Chl*a* is an imperfect proxy of phytoplankton biomass that varies not only with phytoplankton carbon biomass but also with environmental conditions such as light, temperature, or nutrient availability (Babin et al., 1996; Cleveland et al., 1989; Geider et al., 1997). Phytoplankton cells adjust their intracellular Chl*a* in response to changes in light conditions through the process of photoacclimation (Dubinsky & Stambler, 2009; Eisner et al., 2003; Falkowski & Laroche, 1991; Lindley et al., 1995). Photoacclimation-induced variations in intracellular Chl*a* may cause large changes in the Chl*a*-to-carbon ratio (Behrenfeld et al., 2005; Geider, 1987; Sathyendranath et al., 2009) and, thus, changes in the b_{bp}-to-Chl*a* ratio (Behrenfeld & Boss, 2003; Siegel et al., 2005). In the upper oceanic layer of the water column, photoacclimation to high light may result in an increase in the b_{bp}-to-Chl*a* ratio whereas a decrease in this ratio occurs in DCM layers or in the upper layer during winter time in subpolar regimes (NSPG and SO) where photoacclimation to low light occurs.

The impact of light conditions on the b_{bp}:Chl*a* ratio in the different regimes is illustrated in Figure 7. Significant trends are observed in the different layers of the water column for all regimes except for the Black Sea. In the NSPG and SO regimes, the b_{bp}:Chl*a* ratio remains relatively constant with respect to the normalized PAR regardless of the considered layer of the water column (Figures 7a–7c). In contrast, the Mediterranean Sea and the subtropical gyres show a decoupling between b_{bp} and Chl*a* (Figures 5k–5w) so the b_{bp}:Chl*a* ratio in the productive, mixed or surface layer increases with an increase in the normalized PAR (Figures 7a–7c). The seasonal cycle of the b_{bp}:Chl*a* ratio in these regimes results from variations in Chl*a* whereas b_{bp} remains relatively constant over the seasons (not shown). Thus, our results suggest that the variability in the b_{bp}:Chl*a* ratio in the NSPG and SO regimes is not driven at first order by phytoplankton acclimation to light level even if such a process is known to occur at shorter temporal and spatial scales in those regimes (Behrenfeld et al., 2015; Lutz et al., 2003). On the opposite, in both the MED and STG regimes the b_{bp}:Chl*a* ratio variations are essentially driven by phytoplankton photoacclimation.

In these oligotrophic regimes, Chl*a* within the DCM layer is at least a factor of 2 higher than in the productive layer (Figure 6). In the lower part of the euphotic zone, phytoplankton cells hence adjust their intracellular Chl*a* to low light conditions, resulting in a decrease in the b_{bp}:Chl*a* ratio. In addition, the b_{bp}:Chl*a* ratio in this layer seems to remain constant within a regime regardless of absolute light conditions (Figure 7d). Actually, the absolute values of PAR essentially vary between 10 and 25 μmol quanta $m^{-2}\ s^{-1}$ in all the bioregions along the year with values exceeding 50 μmol quanta $m^{-2}\ s^{-1}$ only in the NW_MED and EQNASTZ bioregions. As reported by Letelier et al. (2004) and Mignot et al. (2014), the DCM may follow a given isolume along the seasonal cycle and is thus essentially light driven. Finally, we suggest that the relative homogeneity of both the environmental (PAR) conditions and phytoplankton community composition at the DCM level in subtropical regimes may explain the relative stability of the b_{bp}:Chl*a* values in this water column layer. In the Mediterranean Sea, in contrast, some studies evoke changes in phytoplankton communities in the DCM layer (Crombet et al., 2011) suggesting our results might be further explored when relevant data are available.

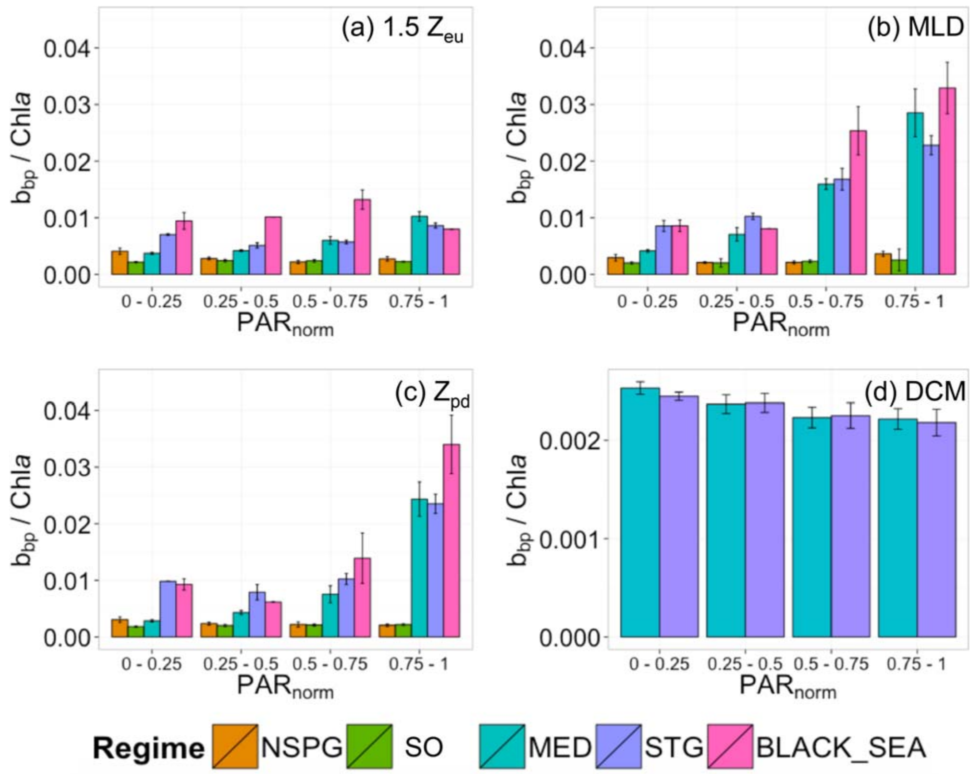

Figure 7. Histogram of the monthly median b_{bp}:Chl*a* ratio as a function of the normalized Photosynthetically Available Radiation (PAR_{norm}) for each regime within (a) the layer comprised between the surface and $1.5Z_{eu}$, (b) the mixed layer, (c) the surface layer, and (d) within the DCM layer. The color code indicates the regimes in which the BGC-Argo data were collected. Note the different *y* scale for Figure 7d compared to Figures 7a–7c. The black lines on the top of each bar represent the standard deviation.

4.4. Variability in the b_{bp}-to-Chl*a* Relationship Is Driven by a Combination of Factors

In the previous sections, we examined the processes that potentially drive the variability in the b_{bp}-to-Chl*a* relationship in the various oceanic regimes considered here.

In the subpolar regimes NSPG and SO, changes in the composition of the particle assemblage, phytoplankton communities in particular, are likely the first-order driver of the seasonal variability in the b_{bp}-to-Chl*a* ratio (Figure 8). In these regimes, the b_{bp}:Chl*a* ratio remains constant regardless of the light intensity in both the productive and surface layers suggesting that phytoplankton photoacclimation is likely not an important driver of the variability in the b_{bp}-to-Chl*a* relationship. We note, however, that in the SO other factors may come into play, such as the light-mixing regime or iron limitation (e.g., Blain et al., 2007, 2013; Boyd, 2002). On the opposite, in the subtropical regime, Chl*a* and b_{bp} are decoupled in the surface layer as well as in the DCM layer. Thus, photoacclimation seems to be the main process driving the vertical and seasonal variability of the b_{bp}-to-Chl*a* relationship, although a varying contribution of nonalgal particles to the particle pool cannot be excluded.

Whereas the subpolar and the subtropical regimes behave as a "biomass regime" and a "photoacclimation regime" (sensu Siegel et al., 2005), respectively, the Mediterranean Sea stands as an intermediate regime between these two end-members. The large number of data available in the Mediterranean allows us to describe this intermediate situation (Figure 8). The Mediterranean Sea appears as a more complex and variable system than the stable and resilient subtropical gyres. Along with the ongoing development of the global BGC-Argo program and associated float deployments, additional data collected in underrepresented regions will become available to make our database more robust and will help to improve our analysis. In the surface layer of the Mediterranean system, a high b_{bp}:Chl*a* ratio in summer might be attributed not only to (i) a background of submicronic living biological cells such as viruses and bacteria or large contribution of nonliving particles including detritus or inorganic particles (Bricaud et al., 2004; Claustre et al., 1999;

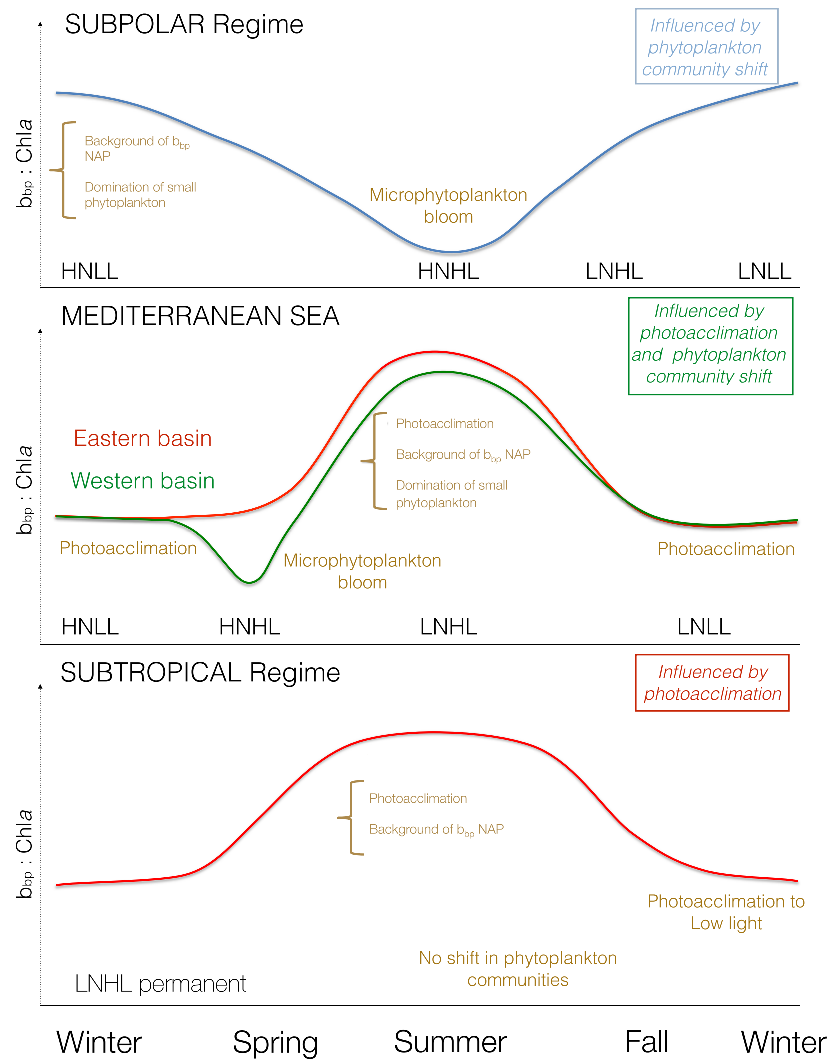

Figure 8. Conceptual scheme of the seasonal cycle of the b_{bp}:Chl*a* ratio in the surface layer of the ocean with potential factors explaining its variability. HNLL, High Nutrient Low Light; HNHL, High Nutrient High Light; LNHL, Low Nutrient High Light; LNLL, Low Nutrient Low Light.

Oubelkheir et al., 2005) or to (ii) photoacclimation of phytoplankton cells to high light conditions as suggested by Bellacicco et al. (2016), but also to (iii) a shift toward small phytoplankton dominated communities (picophytoplankton or nanophytoplankton) after the seasonal microphytoplankton bloom.

Following the longitudinal trophic gradient of the Mediterranean Sea, we observe a variation in the biogeochemical status of the DCM (Figures 1a–d in Supporting information A). The DCM may be attributed to low light photoacclimation similarly to the DCM observed in the STG regime. Yet under favorable light and nutrient conditions encountered in the Western Mediterranean basin, the DCM could result from a real biomass increase occurring at depth instead of a simple photoacclimation "artifact" (Beckmann & Hense, 2007; Cullen, 2014; Mignot et al., 2014; Winn et al., 1995). In such conditions referred to as "deep biomass maximum" (DBM), a concurrent increase in Chl*a* and POC associated with large phytoplankton cells leads to constantly low values of the b_{bp}:Chl*a* ratio (Figure 7d). Our results corroborate previous studies (Crombet et al., 2011; Latasa et al., 1992; Mignot et al., 2014) about the seasonal occurrence of a DBM in the Western Basin of Mediterranean Sea. This deep feature could actually represent a significant source of phytoplankton carbon biomass that is ignored by satellite ocean color sensors that only probe the surface layer of the water column.

5. Conclusions

The main goal of the present study was to examine the variability of the relationship between the particulate backscattering coefficient and the chlorophyll *a* concentration over a broad range of oceanic conditions. Using an extensive BGC-Argo profiling float database, we investigated the sources of variability in this relationship with respect to the vertical dimension as well as on a seasonal and regional scale. In accordance with previous studies (Antoine et al., 2011; Dall'Olmo et al., 2009; Huot et al., 2008; Reynolds et al., 2001; Stramska et al., 2003; Xing et al., 2014) and consistently with the so-called "bio-optical assumption" (Siegel et al., 2005; Smith & Baker, 1978b), a general covariation between b_{bp} and Chl*a* is observed at a global scale in the productive layer of the water column (0–1.5Z_{eu}). Although this covariation seems to be permanent in subpolar regimes in relation with large-amplitude phytoplankton biomass seasonal cycles (Boss & Behrenfeld, 2010; Henson et al., 2006; Lacour et al., 2015), several nuances have been revealed according to the season, considered layer of the water column and bioregion. We suggest that the b_{bp}:Chl*a* ratio, proxy of the C:Chl*a* ratio (Behrenfeld et al., 2015; Westberry et al., 2016), can be used either as an index of the nature (composition and size) of the particle assemblage in a "biomass regime" (NSPG and SO regimes and Western Mediterranean basin) or as a photophysiological index in a "photoacclimation regime" (STG regime and Eastern Mediterranean basin).

The present analysis provides insights into the coupling between major proxies of the POC and phytoplankton biomass in key regimes encountered in the world's open oceans. It points to the strong potential of the recently available global BGC-Argo float database to address regional or seasonal nuances in first-order relationships that have been established in the past on admittedly restricted data sets. In addition, this study stresses out the large variability in the b_{bp}-to-Chl*a* relationship, which is critical to the bio-optical modeling of the b_{bp} coefficient in several semiempirical ocean color models (Garver & Siegel, 1997; Lee et al., 2002; Maritorena et al., 2002). Indeed, bio-optical and reflectance models require detailed knowledge and parameterization of the average trends in the inherent optical properties, especially in open ocean waters where these trends can be related to Chl*a*. Although the analysis of the impact of such variability on ocean color modeling is out of the scope of the present paper, we expect our analysis to be potentially useful in the context of applications to ocean color. Finally, as the amount of BGC-float data will continue to increase, it will be possible to reassess the variability of bio-optical relationships and to establish new "global" standards and regional parameterizations.

Acknowledgments
This paper represents a contribution to the following research projects: remOcean (funded by the European Research Council, grant 246777), NAOS (funded by the Agence Nationale de la Recherche in the frame of the French "Equipement d'avenir" program, grant ANR J11R107-F), the SOCLIM (Southern Ocean and climate) project supported by the French research program LEFE-CYBER of INSU-CNRS, the Climate Initiative of the foundation BNP Paribas and the French polar institute (IPEV), AtlantOS (funded by the European Union's Horizon 2020 Research and Innovation program, grant 2014–633211), E-AIMS (funded by the European Commission's FP7 project, grant 312642), U.K. Bio-Argo (funded by the British Natural Environment Research Council—NERC, grant NE/L012855/1), REOPTIMIZE (funded by the European Union's Horizon 2020 Research and Innovation program, Marie Skłodowska-Curie grant 706781), Argo-Italy (funded by the Italian Ministry of Education, University and Research - MIUR), and the French Bio-Argo program (BGC-Argo France; funded by CNES-TOSCA, LEFE Cyber, and GMMC). We thank the PIs of several BGC-Argo floats missions and projects: Giorgio Dall'Olmo (Plymouth Marine Laboratory, United Kingdom; E-AIMS and U.K. Bio-Argo); Kjell-Arne Mork (Institute of Marine Research, Norway; E-AIMS); Violeta Slabakova (Bulgarian Academy of Sciences, Bulgaria; E-AIMS); Emil Stanev (University of Oldenburg, Germany; E-AIMS); Claire Lo Monaco (Laboratoire d'Océanographie et du Climat: Expérimentations et Approches Numériques); Pierre-Marie Poulain (National Institute of Oceanography and Experimental Geophysics, Italy; Argo-Italy); Sabrina Speich (Laboratoire de Météorologie Dynamique, France; LEFE-GMMC); Virginie Thierry (Ifremer, France; LEFE-GMMC); Pascal Conan (Observatoire Océanologique de Banyuls sur mer, France; LEFE-GMMC); Laurent Coppola (Laboratoire d'Océanographie de Villefranche, France; LEFE-GMMC); Anne Petrenko (Mediterranean Institute of Oceanography, France; LEFE-GMMC); and Jean-Baptiste Sallée (Laboratoire d'Océanographie et du Climat, France; LEFE-GMMC). Collin Roesler (Bowdoin College, USA) and Yannick Huot (University of Sherbrooke, Canada) are acknowledged for useful comments and fruitful discussion. We also thank the International Argo Program and the CORIOLIS project that contribute to make the data freely and publicly available. Data referring to Organelli et al. (2016a; https://doi.org/10.17882/47142) and Barbieux et al. (2017; https://doi.org/10.17882/49388) are freely available on SEANOE.

References

Ahn, Y.-H., Bricaud, A., & Morel, A. (1992). Light backscattering efficiency and related properties of some phytoplankters. *Deep Sea Research Part A. Oceanographic Research Papers*, *39*(11–12), 1835–1855.

Álvarez, E., Morán, X. A. G., López-Urrutia, Á., & Nogueira, E. (2016). Size-dependent photoacclimation of the phytoplankton community in temperate shelf waters (southern Bay of Biscay). *Marine Ecology Progress Series*, *543*, 73–87. https://doi.org/10.3354/meps11580

Antoine, D., Siegel, D. A., Kostadinov, T., Maritorena, S., Nelson, N. B., Gentili, B., . . . Guillocheau, N. (2011). Variability in optical particle backscattering in contrasting bio-optical oceanic regimes. *Limnology and Oceanography*, *56*(3), 955–973. https://doi.org/10.4319/lo.2011.56.3.0955

Babin, M., Morel, A., Fournier-Sicre, V., & Fell, F. (2003). Light scattering properties of marine particles in coastal and open ocean waters as related to the particle mass concentration. *Limnology and Oceanography*, *48*(2), 843–859. https://doi.org/10.4319/lo.2003.48.2.0843

Babin, M., Morel, A., & Gentili, B. (1996). Remote sensing of sea surface Sun-induced chlorophyll fluorescence: Consequences of natural variations in the optical characteristics of phytoplankton and the quantum yield of chlorophyll *a* fluorescence. *International Journal of Remote Sensing*, *17*(12), 2417–2448.

Balch, W. M., Drapeau, D. T., Fritz, J. J., Bowler, B. C., & Nolan, J. (2001). Optical backscattering in the Arabian Sea—Continuous underway measurements of particulate inorganic and organic carbon. *Deep Sea Research Part I: Oceanographic Research Papers*, *48*(11), 2423–2452. https://doi.org/10.1016/S0967-0637(01)00025-5

Balch, W. M., Kilpatrick, K. A., Holligan, P., Harbour, D., & Fernandez, E. (1996a). The 1991 coccolithophore bloom in the central North Atlantic. 2. Relating optics to coccolith concentration. *Limnology and Oceanography*, *41*(8), 1684–1696. https://doi.org/10.4319/lo.1996.41.8.1684

Balch, W. M., Kilpatrick, K. A., & Trees, C. C. (1996b). The 1991 coccolithorphore bloom in the central North Atlantic: I. Optical properties and factors affecting their distribution. *Limnology and Oceanography*, *41*(8), 1669–1683.

Barbieux, M., Organelli, E., Claustre, H., Schmechtig, C., Poteau, A., Boss, E., . . . Xing, X. (2017). *A global database of vertical profiles derived from Biogeochemical Argo float measurements for biogeochemical and bio-optical applications*. SEANOE. https://doi.org/10.17882/49388

Barton, A. D., Lozier, M. S., & Williams, R. G. (2015). Physical controls of variability in North Atlantic phytoplankton communities. *Limnology and Oceanography*, *60*(1), 181–197. https://doi.org/10.1002/lno.10011

Beckmann, A., & Hense, I. (2007). Beneath the surface: Characteristics of oceanic ecosystems under weak mixing conditions—A theoretical investigation. *Progress in Oceanography*, *75*(4), 771–796. https://doi.org/10.1016/j.pocean.2007.09.002

Behrenfeld, M. J., & Boss, E. (2003). The beam attenuation to chlorophyll ratio: An optical index of phytoplankton physiology in the surface ocean? *Deep Sea Research Part I: Oceanographic Research Papers*, *50*(12), 1537–1549. https://doi.org/10.1016/j.dsr.2003.09.002

Behrenfeld, M. J., Boss, E., Siegel, D. A., & Shea, D. M. (2005). Carbon-based ocean productivity and phytoplankton physiology from space. *Global Biogeochemical Cycles*, *19*(1). https://doi.org/10.1029/2004GB002299

Behrenfeld, M. J., O'Malley, R. T., Boss, E. S., Westberry, T. K., Graff, J. R., Halsey, K. H., . . . Brown, M. B. (2015). Revaluating ocean warming impacts on global phytoplankton. *Nature Climate Change*, *6*(3), 323–330. https://doi.org/10.1038/nclimate2838

Bellacicco, M., Volpe, G., Colella, S., Pitarch, J., & Santoleri, R. (2016). Role of photoacclimation on phytoplankton's seasonal cycle in the Mediterranean Sea through satellite ocean color data. *Remote Sensing of Environment*, *184*, 595–604. https://doi.org/10.1016/j.rse.2016.08.004

Biogeochemical-Argo Planning Group. (2016). In H. Claustre & K. Johnson (Eds.), *The scientific rationale, design, and implementation plan for a Biogeochemical-Argo float array* (Report). https://doi.org/10.13155/46601

Birge, R. T. (1939). The propagation of errors. *American Journal of Physics*, *7*(6), 351–357. https://doi.org/10.1119/1.1991484

Bishop, J. K. B. (2009). Autonomous observations of the ocean biological carbon pump. *Oceanography*, *22*(2), 182–193. https://doi.org/10.5670/oceanog.2011.65

Blain, S., Quéguiner, B., Armand, L., Belviso, S., Bombled, B., Bopp, L., . . . Wagener, T. (2007). Effect of natural iron fertilization on carbon sequestration in the Southern Ocean. *Nature*, *446*(7139), 1070–1074. https://doi.org/10.1038/nature05700

Blain, S., Renaut, S., Xing, X., Claustre, H., & Guinet, C. (2013). Instrumented elephant seals reveal the seasonality in chlorophyll and light-mixing regime in the iron-fertilized Southern Ocean. *Geophysical Research Letters*, *40*(24), 6368–6372. https://doi.org/10.1002/2013GL058065

Boss, E., & Behrenfeld, M. (2010). In situ evaluation of the initiation of the North Atlantic phytoplankton bloom. *Geophysical Research Letters*, *37*, L18603. https://doi.org/10.1029/2010GL044174

Boss, E., & Pegau, W. S. (2001). Relationship of light scattering at an angle in the backward direction to the backscattering coefficient. *Applied Optics*, *40*(30), 5503–5507. https://doi.org/10.1364/AO.40.005503

Boyd, P. W. (2002). Environmental factors controlling phytoplankton processes in the Southern Ocean. *Journal of Phycology*, *38*(5), 844–861. https://doi.org/10.1046/j.1529-8817.2002.t01-1-01203.x

Brainerd, K. E., & Gregg, M. C. (1995). Surface mixed and mixing layer depths. *Deep Sea Research Part I: Oceanographic Research Papers*, *42*(9), 1521–1543.

Bricaud, A., Claustre, H., Ras, J., & Oubelkheir, K. (2004). Natural variability of phytoplanktonic absorption in oceanic waters: Influence of the size structure of algal populations. *Journal of Geophysical Research*, *109*(C11). https://doi.org/10.1029/2004JC002419

Bricaud, A., Roesler, C., & Zaneveld, J. R. V. (1995). In situ methods for measuring the inherent optical properties of ocean waters. *Limnology and Oceanography*, *40*(2), 393–410. https://doi.org/10.4319/lo.1995.40.2.0393

Briggs, N., Perry, M. J., Cetinić, I., Lee, C., D'Asaro, E., Gray, A. M., & Rehm, E. (2011). High-resolution observations of aggregate flux during a sub-polar North Atlantic spring bloom. *Deep Sea Research Part I: Oceanographic Research Papers*, *58*(10), 1031–1039. https://doi.org/10.1016/j.dsr.2011.07.007

Brown, C. A., Huot, Y., Werdell, P. J., Gentili, B., & Claustre, H. (2008). The origin and global distribution of second order variability in satellite ocean color and its potential applications to algorithm development. *Remote Sensing of Environment*, *112*(12), 4186–4203. https://doi.org/10.1016/j.rse.2008.06.008

Cetinić, I., Perry, M. J., Briggs, N. T., Kallin, E., D'Asaro, E. A., & Lee, C. M. (2012). Particulate organic carbon and inherent optical properties during 2008 North Atlantic Bloom Experiment. *Journal of Geophysical Research*, *117*(C6). https://doi.org/10.1029/2011JC007771

Cetinić, I., Perry, M. J., D'Asaro, E., Briggs, N., Poulton, N., Sieracki, M. E., & Lee, C. M. (2015). A simple optical index shows spatial and temporal heterogeneity in phytoplankton community composition during the 2008 North Atlantic Bloom Experiment. *Biogeosciences*, *12*(7), 2179–2194. https://doi.org/10.5194/bg-12-2179-2015

Claustre, H., Bishop, J., Boss, E., Bernard, S., Berthon, J.-F., Coatanoan, C., . . . Uitz, J. (2010). *Bio-optical profiling floats as new observational tools for biogeochemical and ecosystem studies: Potential synergies with ocean color remote sensing*. Paper presented at Proceedings of the OceanObs'09: Sustained Ocean Observations and Information for Society Conference, ESA Publication WPP-306, Venice, Italy, September 21–25. https://doi.org/10.5270/OceanObs09.cwp.17

Claustre, H., Morel, A., Babin, M., Cailliau, C., Marie, D., Marty, J.-C., . . . Vaulot, D. (1999). Variability in particle attenuation and chlorophyll fluorescence in the tropical Pacific: Scales, patterns, and biogeochemical implications. *Journal of Geophysical Research*, *104*(C2), 3401–3422.

Claustre, H., Morel, A., Hooker, S. B., Babin, M., Antoine, D., Oubelkheir, K., . . . Maritorena, S. (2002). Is desert dust making oligotrophic waters greener? *Geophysical Research Letters*, *29*(10). https://doi.org/10.1029/2001GL014056

Cleveland, J. S., Perry, M. J., Kiefer, D. A., & Talbot, M. C. (1989). Maximal quantum yield of photosynthesis in the northwest Sargasso Sea. *Journal of Marine Research*, *47*(4), 869–886.

Cokacar, T., Kubilay, N., & Oguz, T. (2001). Structure of Emiliania huxleyi blooms in the Black Sea surface waters as detected by SeaWIFS imagery. *Geophysical Research Letters*, *28*(24), 4607–4610. https://doi.org/10.1029/2001GL013770

Crombet, Y., Leblanc, K., Queguiner, B., Moutin, T., Rimmelin, P., Ras, J., . . . Pujo-Pay, M. (2011). Deep silicon maxima in the stratified oligotrophic Mediterranean Sea. *Biogeosciences*, *8*(2), 459–475. https://doi.org/10.5194/bg-8-459-2011

Cullen, J. J. (1982). The deep chlorophyll maximum: Comparing vertical profiles of chlorophyll *a*. *Canadian Journal of Fisheries and Aquatic Sciences*, *39*(5), 791–803.

Cullen, J. J. (2014). Subsurface chlorophyll maximum layers: Enduring enigma or mystery solved? *Annual Review of Marine Science*, *7*, 207–239. https://doi.org/10.1146/annurev-marine-010213-135111

Dall'Olmo, G., & Mork, K. A. (2014). Carbon export by small particles in the Norwegian Sea. *Geophysical Research Letters*, *41*(8), 2921–2927. https://doi.org/10.1002/2014GL059244

Dall'Olmo, G., Westberry, T. K., Behrenfeld, M. J., Boss, E., & Slade, W. H. (2009). Significant contribution of large particles to optical backscattering in the open ocean. *Biogeosciences*, *6*(6), 947–967. https://doi.org/10.5194/bg-6-947-2009

Dandonneau, Y., Deschamps, P.-Y., Nicolas, J.-M., Loisel, H., Blanchot, J., Montel, Y., . . . Bécu, G. (2004). Seasonal and interannual variability of ocean color and composition of phytoplankton communities in the North Atlantic, equatorial Pacific and South Pacific. *Deep Sea Research Part II: Topical Studies in Oceanography*, *51*(1–3), 303–318. https://doi.org/10.1016/j.dsr2.2003.07.018

de Boyer Montégut, C. (2004). Mixed layer depth over the global ocean: An examination of profile data and a profile-based climatology. *Journal of Geophysical Research*, *109*(C12). https://doi.org/10.1029/2004JC002378

Dickey, T. D. (2003). Emerging ocean observations for interdisciplinary data assimilation systems. *Journal of Marine Systems*, *40–41*, 5–48. https://doi.org/10.1016/S0924-7963(03)00011-3

Dubinsky, Z., & Stambler, N. (2009). Photoacclimation processes in phytoplankton: Mechanisms, consequences, and applications. *Aquatic Microbial Ecology*, *56*(2–3), 163–176. https://doi.org/10.3354/ame01345

Eisner, L. B., Twardowski, M. S., Cowles, T. J., & Perry, M. J. (2003). Resolving phytoplankton photoprotective: Photosynthetic carotenoid ratios on fine scales using in situ spectral absorption measurements. *Limnology and Oceanography*, *48*(2), 632–646. https://doi.org/10.4319/lo.2003.48.2.0632

Falkowski, P. G., & Laroche, J. (1991). Acclimation to spectral irradiance in algae. *Journal of Phycology*, *27*(1), 8–14. https://doi.org/10.1111/j.0022-3646.1991.00008.x

Flory, E. N., Hill, P. S., Milligan, T. G., & Grant, J. (2004). The relationship between floc area and backscatter during a spring phytoplankton bloom. *Deep Sea Research Part I: Oceanographic Research Papers*, *51*(2), 213–223. https://doi.org/10.1016/j.dsr.2003.09.012

Gardner, W. D., Mishonov, A. V., & Richardson, M. J. (2006). Global POC concentrations from in-situ and satellite data. *Deep Sea Research Part II: Topical Studies in Oceanography*, *53*(5–7), 718–740. https://doi.org/10.1016/j.dsr2.2006.01.029

Garver, S. A., & Siegel, D. A. (1997). Inherent optical property inversion of ocean color spectra and its biogeochemical interpretation: 1. Time series from the Sargasso Sea. *Journal of Geophysical Research*, *102*(C8), 607–625.

Geider, R. J. (1987). Light and temperature dependence of the carbon to chlorophyll *a* ratio in microalgae and cyanobacteria: Implications for physiology and growth of phytoplankton. *New Phytologist*, *106*(1), 1–34.

Geider, R. J. (1993). Quantitative phytoplankton physiology: Implications for primary production and phytoplankton growth. *ICES Marine Science Symposium*, *197*, 52–62.

Geider, R. J., MacIntyre, H. L., & Kana, T. M. (1997). Dynamic model of phytoplankton growth and acclimation: Responses of the balanced growth rate and the chlorophyll *a*:carbon ratio to light, nutrient-limitation and temperature. *Marine Ecology Progress Series*, *148*(1–3), 187–200. https://doi.org/10.3354/meps148187

Georges, C., Monchy, S., Genitsaris, S., & Christaki, U. (2014). Protist community composition during early phytoplankton blooms in the naturally iron-fertilized Kerguelen area (Southern Ocean). *Biogeosciences*, *11*(20), 5847–5863. https://doi.org/10.5194/bg-11-5847-2014

Gordon, H. R., & McCluney, W. R. (1975). Estimation of the depth of sunlight penetration in the sea for remote sensing. *Applied Optics*, *14*(2), 413–416. https://doi.org/10.1364/AO.14.000413

Gordon, R., Brown, O. B., Evans, H., Brown, W., Smith, C., Baker, K., & Clark, D. K. (1988). A semianalytic radiance model of ocean color. *Journal of Geophysical Research*, *93*(D9), 10909–10924.

Graff, J. R., Milligan, A. J., & Behrenfeld, M. J. (2012). The measurement of phytoplankton biomass using flow-cytometric sorting and elemental analysis of carbon. *Limnology and Oceanography: Methods*, *10*(11), 910–920. https://doi.org/10.4319/lom.2012.10.910

Graff, J. R., Westberry, T. K., Milligan, A. J., Brown, M. B., Dall'Olmo, G., Van Dongen-Vogels, V., . . . Behrenfeld, M. J. (2015). Analytical phytoplankton carbon measurements spanning diverse ecosystems. *Deep Sea Research Part I: Oceanographic Research Papers*, *102*, 16–25. https://doi.org/10.1016/j.dsr.2015.04.006

Halsey, K. H., & Jones, B. M. (2015). Phytoplankton strategies for photosynthetic energy allocation. *Annual Review of Marine Science*, *7*, 265–297. https://doi.org/10.1146/annurev-marine-010814-015813

Henson, S. A., Robinson, I., Allen, J. T., & Waniek, J. J. (2006). Effect of meteorological conditions on interannual variability in timing and magnitude of the spring bloom in the Irminger Basin, North Atlantic. *Deep Sea Research Part I: Oceanographic Research Papers*, *53*(10), 1601–1615. https://doi.org/10.1016/j.dsr.2006.07.009

Holligan, P. M., Fernández, E., Aiken, J., Balch, W. M., Boyd, P., Burkill, P. H., . . . van der Wal, P. (1993). A biogeochemical study of the coccolithophore, *Emiliania huxleyi*, in the North Atlantic. *Global Biogeochemical Cycles*, *7*(4), 879–900.

Honjo, S., Eglinton, T. I., Taylor, C. D., Ulmer, K. M., Sievert, S. M., Bracher, A., . . . Repeta, D. J. (2014). Understanding the role of the biological pump in the global carbon cycle: An imperative for ocean science. *Oceanography*, *27*(3), 10–16. https://doi.org/10.5670/oceanog.2014.78

Huot, Y., & Antoine, D. (2016). Remote sensing reflectance anomalies in the ocean. *Remote Sensing of Environment*, *184*, 101–111. https://doi.org/10.1016/j.rse.2016.06.002

Huot, Y., Babin, M., Bruyant, F., Grob, C., Twardowski, M. S., Claustre, H., & To, C. (2007). Relationship between photosynthetic parameters and different proxies of phytoplankton biomass in the subtropical ocean. *Biogeosciences*, *4*(5), 853–868. https://doi.org/10.5194/bg-4-853-2007

Huot, Y., Morel, A., Twardowski, M. S., Stramski, D., & Reynolds, R. A. (2008). Particle optical backscattering along a chlorophyll gradient in the upper layer of the eastern South Pacific Ocean. *Biogeosciences*, *5*, 495–507. https://doi.org/10.5194/bg-5-495-2008

IOCCG. (2011). Bio-optical sensors on Argo floats. In H. Claustre (Ed.), *Reports of the International Ocean-Colour Coordinating Group, No. 11*. Dartmouth, Canada.

Johnson, K., & Claustre, H. (2016). Bringing Biogeochemistry into the Argo Age. *Eos, Transactions American Geophysical Union*, 1–7. https://doi.org/10.1029/2016EO062427

Kaufman, Y. J., Koren, I., Remer, L. A., Tanré, D., Ginoux, P., & Fan, S. (2005). Dust transport and deposition observed from the Terra-Moderate Resolution Imaging Spectroradiometer (MODIS) spacecraft over the Atlantic Ocean. *Journal of Geophysical Research*, *110*(D10). https://doi.org/10.1029/2003JD004436

Kiefer, D. A., Diego, S., & Jolla, L. (1973). Chlorophyll *a* fluorescence in marine centric diatoms: Responses of chloroplasts to light and nutrient stress. *Marine Biology*, *23*(1), 39–46.

Kopelevich, O., Burenkov, V., Sheberstov, S., Vazyulya, S., Kravchishina, M., Pautova, L., . . . Grigoriev, A. (2014). Satellite monitoring of coccolithophore blooms in the Black Sea from ocean color data. *Remote Sensing of Environment*, *146*, 113–123. https://doi.org/10.1016/j.rse.2013.09.009

Ku, H. H. (1966). Notes on the use of propagation of error formulas. *Journal of Research of the National Bureau of Standards, Section C: Engineering and Instrumentation*, *70*(4), 263. https://doi.org/10.6028/jres.070C.025

Lacour, L., Claustre, H., Prieur, L., & D'Ortenzio, F. (2015). Phytoplankton biomass cycles in the North Atlantic Subpolar Gyre: A similar mechanism for two different blooms in the Labrador Sea. *Geophysical Research Letters*, *42*, 5403–5410. https://doi.org/10.1002/2015GL064540

Latasa, M., Estrada, M., & Delgado, M. (1992). Plankton pigment relationships in the Northwestern Mediterranean during stratification. *Marine Ecology Progress Series*, *88*, 61–73.

Lee, Z., Carder, K. L., & Arnone, R. A. (2002). Deriving inherent optical properties from water color: A multiband quasi-analytical algorithm for optically deep waters. *Applied Optics*, *41*(27), 5755–5772. https://doi.org/10.1364/AO.41.005755

Legendre, L., Rivkin, R. B., Weinbauer, M. G., Guidi, L., & Uitz, J. (2015). The microbial carbon pump concept: Potential biogeochemical significance in the globally changing ocean. *Progress in Oceanography*, *134*, 432–450. https://doi.org/10.1016/j.pocean.2015.01.008

Letelier, R. M., Karl, D. M., Abbott, M. R., & Bidigare, R. R. (2004). Light driven seasonal patterns of chlorophyll and nitrate in the lower euphotic zone of the North Pacific Subtropical Gyre. *Limnology and Oceanography*, *49*(2), 508–519. https://doi.org/10.4319/lo.2004.49.2.0508

Lewis, M. R., Cullen, J. J., & Platt, T. (1983). Phytoplankton and thermal structure in the upper ocean: Consequences of nonuniformity in chlorophyll profile. *Journal of Geophysical Research: Oceans*, *88*(C4), 2565–2570. https://doi.org/10.1029/JC088iC04p02565

Li, W. K. W. (2002). Macroecological patterns of phytoplankton in the northwestern North Atlantic Ocean. *Nature*, *419*(6903), 154–157. https://doi.org/10.1038/nature00994

Lindley, S. T., Bidigare, R. R., & Barber, R. T. (1995). Phytoplankton photosynthesis parameters along 140°W in the equatorial Pacific. *Deep Sea Research Part II: Topical Studies in Oceanography*, *42*(2–3), 441–463.

Loisel, H., Mériaux, X., Berthon, J.-F., & Poteau, A. (2007). Investigation of the optical backscattering to scattering ratio of marine particles in relation to their biogeochemical composition in the eastern English Channel and southern North Sea. *Limnology and Oceanography*, *52*(2), 739–752. https://doi.org/10.4319/lo.2007.52.2.0739

Loisel, H., & Morel, A. (1998). Light scattering and chlorophyll concentration in case 1 waters: A reexamination. *Limnology and Oceanography*, *43*(5), 847–858. https://doi.org/10.4319/lo.1998.43.5.0847

Loisel, H., Nicolas, J.-M., Deschamps, P.-Y., & Frouin, R. (2002). Seasonal and inter-annual variability of particulate organic matter in the global ocean. *Geophysical Research Letters*, *29*(24). https://doi.org/1029/2002GL015948

Loisel, H., Vantrepotte, V., Norkvist, K., Mériaux, X., Kheireddine, M., Ras, J., . . . Moutin, T. (2011). Characterization of the bio-optical anomaly and diurnal variability of particulate matter, as seen from scattering and backscattering coefficients, in ultra-oligotrophic eddies of the Mediterranean Sea. *Biogeosciences*, *8*(11), 3295–3317. https://doi.org/10.5194/bg-8-3295-2011

Ludwig, W., Dumont, E., Meybeck, M., & Heussner, S. (2009). River discharges of water and nutrients to the Mediterranean and Black Sea: Major drivers for ecosystem changes during past and future decades? *Progress in Oceanography*, *80*(3–4), 199–217. https://doi.org/10.1016/j.pocean.2009.02.001

Lutz, V. A., Sathyendranath, S., Head, E. J. H., & Li, W. K. W. (2003). Variability in pigment composition and optical characteristics of phytoplankton in the Labrador Sea and the Central North Atlantic. *Marine Ecology Progress Series*, *260*, 1–18. https://doi.org/10.3354/meps260001

MacIntyre, H. L., Kana, T. M., Anning, T., & Geider, R. J. (2002). Photoacclimation of photosynthesis irradiance response curves and photosynthetic pigments in microalgae and cyanobacteria. *Journal of Phycology*, *38*(1), 17–38. https://doi.org/10.1046/j.1529-8817.2002.00094.x

Maritorena, S., Siegel, D. A., & Peterson, A. R. (2002). Optimization of a semianalytical ocean color model for global-scale applications. *Applied Optics*, *41*(15), 2705–2714. https://doi.org/10.1364/AO.41.002705

Marty, J. C., & Chiavérini, J. (2010). Hydrological changes in the Ligurian Sea (NW Mediterranean, DYFAMED site) during 1995–2007 and biogeochemical consequences. *Biogeosciences*, *7*(7), 2117–2128. https://doi.org/10.5194/bg-7-2117-2010

Mayot, N., D'Ortenzio, F., D'Alcalà, M. R., Lavigne, H., & Claustre, H. (2016). Interannual variability of the Mediterranean trophic regimes from ocean color satellites. *Biogeosciences*, *13*(6), 1901–1917. https://doi.org/10.5194/bg-13-1901-2016

Mendes, C. R. B., Kerr, R., Tavano, V. M., Cavalheiro, F. A., Garcia, C. A. E., Dessai, D. R. G., & Anilkumar, N. (2015). Cross-front phytoplankton pigments and chemotaxonomic groups in the Indian sector of the Southern Ocean. *Deep Sea Research Part II: Topical Studies in Oceanography*, *118*, 221–232. https://doi.org/10.1016/j.dsr2.2015.01.003

Mignot, A., Claustre, H., Uitz, J., Poteau, A., D'Ortenzio, F., & Xing, X. (2014). Understanding the seasonal dynamics of phytoplankton biomass and the deep chlorophyll maximum in oligotrophic environments: A Bio-Argo float investigation. *Global Biogeochemical Cycles*, *28*, 1–21. https://doi.org/10.1002/2013GB004781

Mitchell, B. G. (1992). Predictive bio-optical relationships for polar oceans and marginal ice zones. *Journal of Marine Systems*, *3*(1–2), 91–105. https://doi.org/10.1016/0924-7963(92)90032-4

Mitchell, B. G., & Holm-Hansen, O. (1991). Bio-optical properties of Antarctic Peninsula waters: Differentiation from temperate ocean models. *Deep Sea Research Part A. Oceanographic Research Papers*, *38*(8–9), 1009–1028. https://doi.org/10.1016/0198-0149(91)90094-V

Morel, A., & Ahn, Y. (1991). Optics of heterotrophic nanoftagellates and ciliates: A tentative assessment of their scattering role in oceanic waters compared to those of bacterial and algal cells. *Journal of Marine Research*, *49*(1), 177–202.

Morel, A., & Berthon, J.-F. (1989). Surface pigments, algal biomass profiles, and potential production of the euphotic layer: Relationships reinvestigated in view of remote-sensing applications. *Limnology and Oceanography*, *34*(8), 1545–1562. https://doi.org/10.4319/lo.1989.34.8.1545

Morel, A., & Bricaud, A. (1986). Inherent optical properties of algal cells including picoplankton: Theorical and experimental results. *Canadian Bulletin of Fisheries and Aquatic Sciences*, *214*, 521–559.

Morel, A., Claustre, H., Antoine, D., & Gentili, B. (2007). Natural variability of bio-optical properties in Case 1 waters: Attenuation and reflectance within the visible and near-UV spectral domains, as observed in South Pacific and Mediterranean waters. *Biogeosciences*, *4*(4), 913–925. https://doi.org/10.5194/bg-4-913-2007

Morel, A., & Maritorena, S. (2001). Bio-optical properties of oceanic waters: A reappraisal. *Journal of Geophysical Research*, *106*(C4), 7163–7180. https://doi.org/10.1029/2000JC000319

Navarro, G., Alvain, S., Vantrepotte, V., & Huertas, I. E. (2014). Identification of dominant phytoplankton functional types in the Mediterranean Sea based on a regionalized remote sensing approach. *Remote Sensing of Environment*, *152*, 557–575. https://doi.org/10.1016/j.rse.2014.06.029

Organelli, E., Barbieux, M., Claustre, H., Schmechtig, C., Poteau, A., Bricaud, A., . . . Dall'Olmo, G. (2016a). *A global bio-optical database derived from Biogeochemical Argo float measurements within the layer of interest for field and remote ocean colour applications*. SEANOE. https://doi.org/10.17882/47142

Organelli, E., Barbieux, M., Claustre, H., Schmechtig, C., Poteau, A., Bricaud, A., . . . Xing, X. (2017b). Two databases derived from BGC-Argo float measurements for marine biogeochemical and bio-optical applications. *Earth System Science Data*, *9*, 861–880. https://doi.org/10.5194/essd-9-861-2017

Organelli, E., Claustre, H., Bricaud, A., Schmechtig, C., Poteau, A., Xing, X., . . . Vellucci, V. (2016b). A novel near real-time quality-control procedure for radiometric profiles measured by Bio-Argo floats: Protocols and performances. *Journal of Atmospheric and Oceanic Technology*, *33*, 937–951. https://doi.org/10.1175/JTECH-D-15-0193.1

Organelli, E., Claustre, H., Bricaud, A., Barbieux, M., Uitz, J., D'Ortenzio, F. & Dall'Olmo, G. (2017a). Bio-optical anomalies in the world's oceans: An investigation on the diffuse attenuation coefficients for downward irradiance derived from Biogeochemical Argo float measurements. *Journal of Geophysical Research: Oceans*, *122*, 3543–3564. https://doi.org/10.1002/2016JC012629

Oubelkheir, K., Claustre, H., Sciandra, A., & Babin, M. (2005). Bio-optical and biogeochemical properties of different trophic regimes in oceanic waters. *Limnology and Oceanography*, *50*(6), 1795–1809. https://doi.org/10.4319/lo.2005.50.6.1795

Proctor, C. W., & Roesler, C. S. (2010). New insights on obtaining phytoplankton concentration and composition from in situ multispectral Chlorophyll fluorescence. *Limnology and Oceanography: Methods*, *8*(12), 695–708. https://doi.org/10.4319/lom.2010.8.695

Prospero, J. M. (1996). The atmospheric transport of particles to the ocean. *SCOPE—Scientific Committee on Problems of the Environment, International Council of Scientific Unions*, *57*, 19–52.

Ras, J., Claustre, H., & Uitz, J. (2008). Spatial variability of phytoplankton pigment distributions in the Subtropical South Pacific Ocean: Comparison between in situ and predicted data. *Biogeosciences*, *5*(2), 353–369. https://doi.org/10.5194/bg-5-353-2008

Reynolds, R. A., Stramski, D., & Mitchell, B. G. (2001). A chlorophyll-dependent semianalytical reflectance model derived from field measurements of absorption and backscattering coefficients within the Southern Ocean. *Journal of Geophysical Research*, *106*(C4), 7125–7138. https://doi.org/10.1029/1999JC000311

Riser, S. C., & Johnson, K. S. (2008). Net production of oxygen in the subtropical ocean. *Nature*, *451*(7176), 323–325. https://doi.org/10.1038/nature06441

Roesler, C., Uitz, J., Claustre, H., Boss, E., Xing, X., Organelli, E., . . . Barbieux, M. (2017). Recommendations for obtaining unbiased chlorophyll estimates from in situ chlorophyll fluorometers: A global analysis of WET Labs ECO sensors. *Limnology and Oceanography: Methods*, *15*(6), 572–585. https://doi.org/10.1002/lom3.10185

Roesler, C. S., & Barnard, A. H. (2013). Optical proxy for phytoplankton biomass in the absence of photophysiology: Rethinking the absorption line height. *Methods in Oceanography*, *7*, 79–94. https://doi.org/10.1016/j.mio.2013.12.003

Sammartino, M., Di Cicco, A., Marullo, S., & Santoleri, R. (2015). Spatio-temporal variability of micro-, nano- and pico-phytoplankton in the Mediterranean Sea from satellite ocean colour data of SeaWiFS. *Ocean Science*, *11*(5), 759–778. https://doi.org/10.5194/os-11-759-2015

Sathyendranath, S., Stuart, V., Nair, A., Oka, K., Nakane, T., Bouman, H., . . . Platt, T. (2009). Carbon-to-chlorophyll ratio and growth rate of phytoplankton in the sea. *Marine Ecology Progress Series*, *383*, 73–84. https://doi.org/10.3354/meps07998

Schmechtig, C., Claustre, H., Poteau, A., & D'Ortenzio, F. (2014). *Bio-Argo quality control manual for the chlorophyll-a concentration* (p. 1–13). Argo Data Management. https://doi.org/10.13155/35385

Schmechtig, C., Poteau, A., Claustre, H., D'Ortenzio, F., Dall'Olmo, G., & Boss, E. (2016). *Processing Bio-Argo particle backscattering at the DAC level Version* (p. 1–13). Argo Data Management. https://doi.org/10.13155/39459

Siegel, D. A., Behrenfeld, M. J., Maritorena, S., McClain, C. R., Antoine, D., Bailey, S. W., . . . Yoder, J. A. (2013). Regional to global assessments of phytoplankton dynamics from the SeaWiFS mission. *Remote Sensing of Environment*, *135*, 77–91. https://doi.org/10.1016/j.rse.2013.03.025

Siegel, D. A., Maritorena, S., Nelson, N. B., & Behrenfeld, M. J. (2005). Independence and interdependencies among global ocean color properties: Reassessing the bio-optical assumption. *Journal of Geophysical Research*, *110*(C7). https://doi.org/10.1029/2004JC002527

Siokou-Frangou, I., Christaki, U., Mazzocchi, M. G., Montresor, M., Ribera D'Alcalá, M., Vaqué, D., & Zingone, A. (2010). Plankton in the open Mediterranean Sea: A review. *Biogeosciences*, *7*(5), 1543–1586. https://doi.org/10.5194/bg-7-1543-2010

Smith, R. C., & Baker, K. S. (1978a). Optical classification of natural waters. *Limnology and Oceanography*, *23*(2), 260–267. https://doi.org/10.4319/lo.1978.23.2.0260

Smith, R. C., & Baker, K. S. (1978b). The bio-optical state of ocean waters and remote sensing. *Limnology and Oceanography*, *23*(2), 247–259. https://doi.org/10.4319/lo.1978.23.2.0247

Staehr, P. A., Henriksen, P., & Markager, S. (2002). Photoacclimation of four marine phytoplankton species to irradiance and nutrient availability. *Marine Ecology Progress Series*, *238*, 47–59. https://doi.org/10.3354/meps238047

Stramska, M., Stramski, D., Hapter, R., Kaczmarek, S., & Ston, J. (2003). Bio-optical relationships and ocean color algorithms for the north polar region of the Atlantic. *Journal of Geophysical Research*, *108*(C5), 2156–2202. https://doi.org/10.1029/2001JC001195

Stramski, D., Boss, E., Bogucki, D., & Voss, K. J. (2004). The role of seawater constituents in light backscattering in the ocean. *Progress in Oceanography*, *61*(1), 27–56. https://doi.org/10.1016/j.pocean.2004.07.001

Stramski, D., Bricaud, A., & Morel, A. (2001). Modeling the inherent optical properties of the ocean based on the detailed composition of the planktonic community. *Applied Optics*, *40*(18), 2929–2945. https://doi.org/10.1364/AO.40.002929

Stramski, D., Reynolds, R. A., Babin, M., Kaczmarek, S., Lewis, M. R., Röttgers, R., . . . Claustre, H. (2008). Relationships between the surface concentration of particulate organic carbon and optical properties in the eastern South Pacific and eastern Atlantic Oceans. *Biogeosciences*, *5*(1), 171–201. https://doi.org/10.5194/bg-5-171-2008

Stramski, D., Reynolds, R. A., Kahru, M., & Mitchell, B. G. (1999). Estimation of particulate organic carbon in the ocean from satellite remote sensing. *Science*, *285*(5425), 239–242.

Sullivan, J., Twardowski, M., Ronald, S., Zaneveld, J. V., & Moore, C. C. (2013). Measuring optical backscattering in water. In A. A. Kokhanovsky (Ed.), *Light scattering reviews 7*, 189–224. Berlin, Germany: Springer.

Szeto, M., Werdell, P. J., Moore, T. S., & Campbell, J. W. (2011). Are the world's oceans optically different? *Journal of Geophysical Research*, *116*(C7). https://doi.org/10.1029/2011JC007230

Tanhua, T., Hainbucher, D., Schroeder, K., Cardin, V., Álvarez, M., & Civitarese, G. (2013). The Mediterranean Sea system: A review and an introduction to the special issue. *Ocean Science*, *9*(5), 789–803. https://doi.org/10.5194/os-9-789-2013

Taylor, J. R., & Ferrari, R. (2010). Buoyancy and wind-driven convection at mixed layer density fronts. *Journal of Physical Oceanography*, *40*(6), 1222–1242. https://doi.org/10.1175/2010JPO4365.1

Uitz, J., Claustre, H., Griffiths, F. B., Ras, J., Garcia, N., & Sandroni, V. (2009). A phytoplankton class-specific primary production model applied to the Kerguelen Islands region (Southern Ocean). *Deep Sea Research Part I: Oceanographic Research Papers*, *56*(4), 541–560. https://doi.org/10.1016/j.dsr.2008.11.006

Uitz, J., Claustre, H., Morel, A., & Hooker, S. B. (2006). Vertical distribution of phytoplankton communities in open ocean: An assessment based on surface chlorophyll. *Journal of Geophysical Research*, *111*(C8). https://doi.org/10.1029/2005JC003207

Vaillancourt, R. D., Brown, C. W., Guillard, R. R. L., & Balch, W. M. (2004). Light backscattering properties of marine phytoplankton: Relationships to cell size, chemical composition and taxonomy. *Journal of Plankton Research*, *26*(2), 191–212. https://doi.org/10.1093/plankt/fbh012

Volk, T., & Hoffert, M. I. (1985). Ocean carbon pumps: Analysis of relative strengths and efficiencies in ocean-driven atmospheric CO_2 changes. In E. T. Sundquist & W. S. Broecker (Eds.), *The carbon cycle and atmospheric CO2: Natural variations Archean to present, geophysical monograph series* (Vol. 32, pp. 99–110). Washington, DC: American Geophysical Union.

Westberry, T. K., Schultz, P., Behrenfeld, M. J., Dunne, J. P., Hiscock, M. R., Maritorena, S., . . . Siegel, D. A. (2016). Annual cycles of phytoplankton biomass in the subarctic Atlantic and Pacific Ocean. *Global Biogeochemical Cycles*, *30*(2), 175–190. https://doi.org/10.1002/2015GB005276

Whitmire, A. L., Pegau, W. S., Karp-Boss, L., Boss, E., & Cowles, T. J. (2010). Spectral backscattering properties of marine phytoplankton cultures. *Optics Express*, *18*(14), 15073–15093. https://doi.org/10.1364/OE.18.015073

Winn, C. D., Campbell, L., Christian, J. R., Letelier, R. M., Hebel, D. V., Dore, J. E., . . . Karl, D. M. (1995). Seasonal variability in the phytoplankton community of the North Pacific Subtropical Gyre. *Global Biogeochemical Cycles*, *9*(4), 605–620. https://doi.org/10.1029/95GB02149

Wong, A., Keeley, R., & Carval, T. (2013). *Argo quality control manual* (p. 1–50). Argo Data Management. https://doi.org/10.13155/33951

Xing, X., Claustre, H., Blain, S., D'Ortenzio, F., Antoine, D., Ras, J., & Guinet, C. (2012). Quenching correction for in vivo chlorophyll fluorescence acquired by autonomous platforms: A case study with instrumented elephant seals in the Kerguelen region (Southern Ocean). *Limnology and Oceanography*, *10*(7), 483–495. https://doi.org/10.4319/lom.2012.10.483

Xing, X., Claustre, H., Boss, E., Roesler, C., Organelli, E., Poteau, A., . . . D'Ortenzio, F. (2016). Correction of profiles of in-situ chlorophyll fluorometry for the contribution of fluorescence originating from non-algal matter. *Limnology and Oceanography: Methods*, *15*(1), 80–93. https://doi.org/10.1002/lom3.10144

Xing, X., Claustre, H., Uitz, J., Mignot, A., Poteau, A., & Wang, H. (2014). Seasonal variations of bio-optical properties and their interrelationships observed by Bio-Argo floats in the subpolar North Atlantic. *Journal of Geophysical Research: Oceans*, *119*(10), 7372–7388. https://doi.org/10.1002/2014JC010189

Xing, X., Morel, A., Claustre, H., Antoine, D., D'Ortenzio, F., Poteau, A., & Mignot, A. (2011). Combined processing and mutual interpretation of radiometry and fluorimetry from autonomous profiling Bio-Argo floats: Chlorophyll *a* retrieval. *Journal of Geophysical Research*, *116*(C6). https://doi.org/10.1029/2010JC006899

Yentsch, C. S., & Phinney, D. A. (1989). A bridge between ocean optics and microbial ecology. *Limnology and Oceanography*, *34*(8), 1694–1705. https://doi.org/10.4319/lo.1989.34.8.1694

Zhang, X., Hu, L., & He, M.-X. (2009). Scattering by pure seawater: Effect of salinity. *Optics Express*, *17*(7), 5698–5710. https://doi.org/10.1364/OE.17.012685